Hydraulic Radial Piston Motor

Introduction and Design Objectives

Hydraulic motors are widely used in industrial, mobile, and energy systems where high torque at low rotational speeds is required. Their ability to convert hydraulic pressure into mechanical rotation makes them particularly suitable for applications such as heavy machinery, winches, drilling equipment, and propulsion systems. Among the various configurations available, radial piston motors are commonly employed due to their high torque density, compact structure, and efficient mechanical leverage.

A radial piston motor operates through the interaction between multiple pistons arranged radially around a central cam or eccentric ring. As pressurised fluid is supplied to the system, the pistons undergo reciprocating motion and transmit force to the cam surface, producing continuous rotational output. This direct coupling between hydraulic pressure and mechanical motion allows for efficient energy conversion but also introduces inherent dynamic complexity.

The performance of these systems is governed by tightly coupled interactions between geometry, fluid flow, and mechanical motion. In particular, the cam/eccentric profile defines piston displacement kinematics, which directly influences chamber volume variation and therefore pressure evolution within the hydraulic system. Additionally, the discrete nature of piston engagement introduces periodic fluctuations in both force and torque output.

A key challenge in radial piston motor design is the presence of torque ripple and pressure fluctuations. These arise due to non-uniform piston actuation, time-varying chamber volumes, and the compressibility of the working fluid. Together, these effects lead to oscillatory behaviour in the system output, which can contribute to increased vibration, acoustic noise, reduced efficiency, and long-term mechanical fatigue.

The design of radial piston motors is therefore inherently a multi-domain engineering problem involving trade-offs between hydraulic performance, mechanical efficiency, and dynamic stability. Improvements in one aspect of performance may negatively impact others, making systematic analysis and optimisation essential.

The aim of this project is to develop a physics-based model of a radial piston motor that captures the coupled relationship between geometry, hydraulics, and mechanical torque generation. This model is used to analyse system behaviour and evaluate performance in terms of torque ripple, pressure variation, and efficiency. The results are then used to support design evaluation and optimisation of key system parameters.

Concept Designs and Architecture Selection

Radial piston motors are realised in several distinct mechanical architectures, each with different implications for torque density, manufacturability, efficiency, and durability. For this project, four common configurations are considered:

– Eccentric Shaft
– Cam Ring
– Crankshaft
– Phased Rotor

These architectures are evaluated against the project constraints: high torque at low speed, low torque ripple, good efficiency, manageable cost/complexity, and suitability for detailed multi-physics modelling and optimisation.

Table 1: Design Criteria and Individual Weightings

Criteria	**Eccentric**	**Cam Ring**	**Crankshaft**	**Phased Rotor**
Torque Smoothness	Very Low	Moderate	Moderate–High	Very High
Pressure Stability	Moderate	Moderate–High	High	Moderate–High
Structural Simplicity	High	Moderate–High	Moderate	Low
Durability	Moderate	High	Moderate–High	High
Efficiency	Low	Moderate–High	Moderate–High	High
Packaging Efficiency	High	Moderate–High	Moderate	Moderate
Manufacturing Ease	High	Moderate–High	Moderate	Low
Control Simplicity	High	Moderate	Moderate	Low
Thermal Performance	Low	Moderate–High	Moderate–High	High
Tolerance Robustness	Low	High	Moderate	Moderate
Optimisation Suitability	Moderate	High	Low	Moderate

Eccentric Shaft

In the eccentric shaft design, pistons act directly on an offset shaft. This architecture is mechanically simple, compact, and relatively easy to manufacture. However, the eccentric profile is typically limited in shape, and torque ripple reduction relies mainly on piston count and phasing rather than sophisticated profile shaping. The direct loading of the shaft also introduces bending and bearing loads that complicate high-pressure, long-life operation along with the high friction and hertzian stresses from direct contact of the pistons on the housing wall. Consequently, while attractive for simplicity, this architecture is low on efficiency and lifespan which makes it very undesirable though simple to optimize.

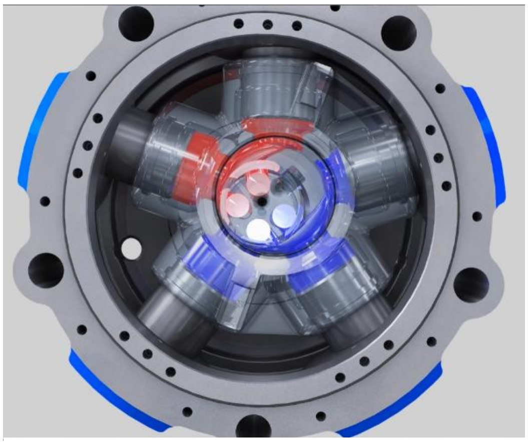

Figure 1: CAD drawing of Eccentric Shaft Design

Cam Ring

The cam ring-type radial piston motor employs a multi-lobe cam profile that governs piston motion. This configuration allows multiple pistons to contribute to torque generation simultaneously, significantly reducing torque ripple. Additionally, the rolling contact between pistons and the cam

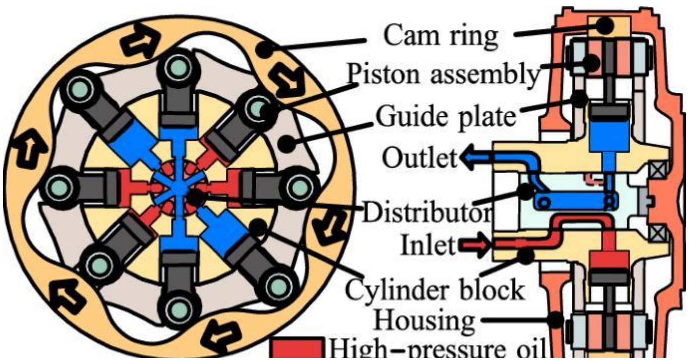

Figure 2: Cam Ring Design Drawing

surface reduces friction losses and improves overall efficiency. This type of motor is widely used in high-pressure, high-torque industrial applications.

Crankshaft

The crankshaft-type motor features a simple mechanical configuration in which pistons are connected to a crankshaft via connecting rods. This design is widely used due to its ease of manufacturing, low cost, and well-established design methodology. However, its torque output is inherently non-uniform due to the limited number of pistons engaged at any given time. This results in significant torque ripple and vibration, particularly under high-pressure conditions.

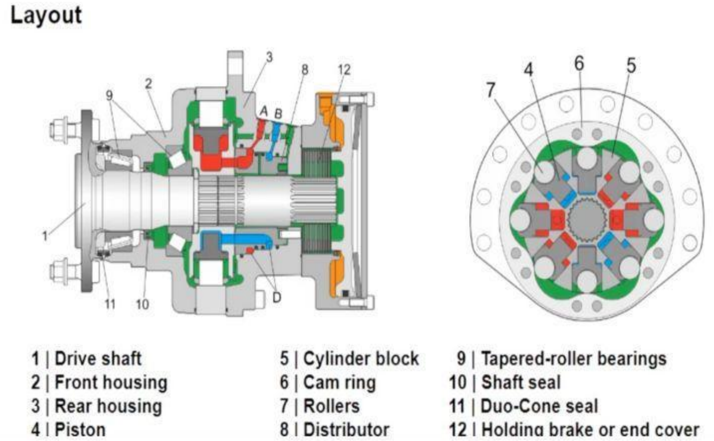

Figure 3: Crankshaft Design Drawing

Phased Rotor

Phased – Rotor architectures can significantly reduce torque ripple by superimposing multiple torque waveforms. They offer excellent smoothness and high torque capacity, but at the cost of increased size, mass, and mechanical complexity. Synchronisation, sealing, and structural stiffness become more challenging, and the design space grows substantially, making optimisation more expensive and less transparent. The risks of cavitation, high frequency pressure ripple, hydraulic short circuiting and motor lockup all drastically increase compared to the much simpler single rotor cam design making it far less reliable for a simple application where the best performance is not necessary.

Figure 4: CAD Drawing of the Phased Rotor Design

Selected Architecture

Using the above criteria and comparative weightings, this following design matrix table was constructed to represent the differing priorities of the criteria.

Table 2: Design Matrix with Priority Adjusted Results

Criteria	**Weights**	**Eccentric**		**Cam Ring**		**Crankshaft**		**Phased Rotor**	
Torque Smoothness	5	1	5	3	15	4	20	6	30
Pressure Stability	3	3	9	4	12	5	15	4	12
Structural Simplicity	2	5	10	4	8	3	6	2	4
Durability	3	3	9	5	15	4	12	5	12
Efficiency	3	2	6	4	12	4	12	5	12

Packaging Efficiency	2	5	10	4	8	3	6	3	6
Manufacturing Ease	4	5	20	4	16	3	12	2	8
Control Simplicity	3	5	15	3	9	3	9	2	6
Thermal Performance	3	2	6	4	12	4	12	5	15
Tolerance Robustness	2	2	4	5	10	3	6	3	6
Optimisation Suitability	1	3	3	5	5	2	2	3	3
Total			97		122		112		114

Given the project objectives – minimising torque ripple via geometric and timing optimisation, maximising efficiency through detailed control of contact and lubrication, and ensuring durability under high-pressure, high-cycle operation – and the results of the selection matrix above, the cam ring architecture is the most suitable choice. It provides:

- A rich, continuous design space for cam profile optimisation
- A stiff, compact structure that supports precise control of clearances and contact geometry
- Good compatibility with EHL, fatigue, and thermal modelling
- A clear mapping between design parameters and performance metrics for the ML-driven optimiser

The subsequent modelling and optimisation work will therefore focus on a cam ring radial piston motor, with the other architectures serving primarily as reference points for comparison.

Mathematical Modelling of the Hydraulic Motor System

The mathematical model developed in this work provides a reduced-order but physically representative description of the coupled geometry, kinematics, fluid dynamics, and mechanical force transmission within a radial piston hydraulic motor. The purpose of this model is to capture the dominant physical mechanisms that influence torque ripple, pressure pulsation, and overall efficiency while remaining computationally tractable for use within an optimisation loop. The modelling framework adopts a periodic steady-state perspective, reflecting the inherently cyclic nature of cam-driven piston motion, and incorporates key nonlinearities such as fluid compressibility, port flow characteristics, and geometric coupling. This section outlines the governing equations, modelling assumptions, and frequency-domain formulation used to evaluate motor performance. The overarching system model is a sequential nonlinear mapping:

$$x \rightarrow C(\theta) \rightarrow s(\theta) \rightarrow P(\theta) \rightarrow \tau(\theta)$$

where:

x: design vector (cam geometry, piston count, hydraulic parameters, leakage, clearances, porting)

$C(\theta)$: cam profile

$s(\theta)$: piston displacement

$P(\theta)$: chamber pressure

$\tau(\theta)$: output torque

The objective of the model is to predict and minimise torque ripple through a frequency-domain representation of the coupled nonlinear dynamics.

Modelling Assumptions

To ensure clarity and reproducibility, the following assumptions are applied throughout the modelling framework:

1. **Fluid Compressibility:** The hydraulic fluid is treated as weakly compressible with a constant bulk modulus β. Thermal effects on compressibility are neglected.
2. **Isothermal Conditions:** All processes are assumed isothermal. Temperature-dependent viscosity and density variations are not modelled.
3. **Rigid-Body Mechanics:** Pistons, cam surfaces, and the housing are assumed rigid. Elastic deformation and structural compliance are neglected.
4. **Linear Leakage Model:** Leakage is represented using a linear pressure-dependent term $Q_{\text{leak}} = C_l(P - P_t)$. Turbulent or nonlinear leakage effects are not included.
5. **Constant Discharge Coefficient:** The port flow coefficient $C_d$is assumed constant, independent of Reynolds number or cavitation effects.
6. **Quasi-Static Cam Rotation:** Shaft rotational speed $\omega$is assumed constant, and dynamic torsional oscillations are neglected.
7. **Negligible Valve Plate Dynamics:** Valve plate motion is not modelled; only its geometric timing and overlap functions are considered.

These assumptions define the validity range of the model and ensure that the resulting equations remain analytically and computationally manageable.

Cam Geometry and Kinematics

The cam profile is defined using a periodic B-spline:

$$C(\theta) = \sum_{i=0}^{n} N_{i,p}(\theta)P_i$$

with periodic constraints:

$$P_0 = P_n, C(0) = C(2\pi)$$

Radial displacement:

$$s(\theta) = \| C(\theta) \|$$

Velocity and acceleration:

$$s' = \omega \frac{ds}{d\theta}, \qquad s'' = \omega^2 \frac{d^2 s}{d\theta^2}$$

Jerk (used as smoothness constraint):

$$s''' = \omega^3 \frac{d^3 s}{d\theta^3}$$

Hydraulic System

Chamber Volume Dynamics

Each piston chamber volume evolves as:

$$V(\theta) = V_{dead} + A_p s(\theta)$$

Time derivative:

$$\frac{dV}{dt} = A_p \dot{s}$$

Compressible Hydraulic Dynamics

Mass conservation:

$$\frac{dV}{dt} = Q_{in} - Q_{out} - Q_{leak}$$

Using bulk modulus:

$$\beta = -V \frac{dP}{dV}$$

Pressure dynamics:

$$\frac{dP}{dt} = \frac{\beta}{V(\theta)} \left(Q_{in} - Q_{out} - Q_{leak} - A_p \dot{s} \right)$$

Flow Relations

The effective port area is defined as:

$$A(\theta) = A_{port} \cdot \alpha(\theta)$$

where:

- $A_{port}$is the nominal geometric port area
- $\alpha(\theta) \in [0,1]$is the non-dimensional overlap function

For a valve plate consisting of N_p discrete ports with angular spacing:

$$\theta_p = \theta_{shift} + p \frac{2\pi}{N_p}, \qquad p = 1, \dots, N_p$$

the overlap function is approximated as a linear windowing function:

$$\alpha(\theta) = \sum_{p=1}^{N_{ports}} \max\left(0,1 - \frac{\mid \theta - \theta_p \mid}{\Delta\theta_p/2}\right)$$

where $\Delta\theta_p$is the angular span of port p.

The port flow is then:

$$Q_{port} = C_d A(\theta) \sqrt{\frac{2 \mid P_s - P \mid}{\rho}}$$

With leakage:

$$Q_{leak} = C_l(P - P_t)$$

Thus, the linearised flow model:

$$Q_{net} \approx Q_0 + C_f(P - P_0)$$

Linearised Pressure Dynamics

This form is the control-relevant reduced hydraulic subsystem.

$$\frac{dP}{dt} + \frac{\beta C_f}{V} P = \frac{\beta C_f}{V} P_s - \frac{\beta A_p}{V} \dot{s}$$

The pressure evolution equation indicates that chamber pressure increases when the net inflow exceeds the volumetric expansion caused by piston motion. Conversely, pressure decreases when the piston retracts faster than fluid can enter the chamber. The bulk modulus term acts as an effective hydraulic stiffness, linking volume change directly to pressure variation.

Mechanical Dynamics

Due to the compressible nature of the hydraulic fluid, the system behaves like a mass-spring-damper, thus the force balance on piston is:

$$m_p s'' + c_f s' + F_{fric} = A_p P$$

Rearranged:

$$m_p s'' = A_p P - c_f \dot{s} - F_{load}$$

Emergent Hydraulic Stiffness

From compressibility:

$$k_f = \frac{\beta A_p^2}{V_{eq}}$$

This yields equivalent form:

$$m_p s'' + c_f s' + k_f s = F_{hyd}$$

With natural frequency:

$$\omega_n = \sqrt{\frac{k_f}{m_p}}$$

And damping ratio:

$$\zeta = \frac{c_f}{2\sqrt{m_p k_f}}$$

The mechanical force balance shows that piston acceleration results from the difference between hydraulic force and resistive forces such as viscous damping and friction. This formulation highlights the mass-spring-damper behaviour inherent in compressible hydraulic systems, where fluid stiffness and piston inertia interact to produce oscillatory dynamics.

Frequency-Domain Representation

Torque ripple and pressure pulsation are inherently periodic phenomena arising from the cyclic interaction between pistons and cam lobes. Representing these signals using Fourier series enables direct quantification of harmonic content, which is strongly correlated with vibration, noise, and perceived smoothness. Low-order harmonics dominate mechanical response and are therefore the primary target for reduction. Truncating the series to a finite number of harmonics Ncaptures all physically relevant ripple components while maintaining computational efficiency.

Periodic signals are expressed as:

$$x(\theta) = \sum_{n=0}^{\infty} \hat{x}_n \, e^{in\theta}$$

Pressure Harmonics:

$$\hat{P}_n = \frac{-\beta A_p / V}{in\omega + \beta C_f / V} \; \hat{s}_n$$

Torque Harmonics:

$$\hat{\tau}_n = \Gamma_n \left(A_p \hat{P}_n + m_p \omega^2 n^2 \hat{s}_n \right)$$

Low-order harmonics correspond to perceptible oscillations in shaft torque, while higher-order components are typically attenuated by inertia and damping. This representation is essential for defining ripple metrics and optimisation objectives.

Optimization Framework

The objective is to determine an optimal design vector:

$$x = \{C(\theta), A_{port}, A_{leak}, c_{clear}, \dots\}$$

such that system performance is improved across competing objectives:

- minimise torque ripple
- minimise pressure ripple
- maximise efficiency
- satisfy mechanical and hydraulic constraints
- minimise cost (tolerances)

Thus, the optimization problem can be framed as:

$$\min_{x} J(x) \ \text{ s.t. } g_i(x) \leq 0$$

Ripple Metrics

Pressure ripple:

$$R_P = \frac{\sqrt{\sum_{n=1}^{N} |\hat{P}_n|^2}}{|\hat{P}_0|}$$

Torque ripple:

$$R_\tau = \frac{\sqrt{\sum_{n=1}^{N} |\hat{\tau}_n|^2}}{|\hat{\tau}_0|}$$

Unified Spectral Objective Function

Instead of separating pressure and torque, combine them in one function:

$$J_{spec} = \sum_{n=1}^{N} \left(w_P |\hat{P}_n|^2 + w_\tau |\hat{\tau}_n|^2 \right)$$

This represents total harmonic energy content across system outputs.

Efficiency and Losses

Efficiency:

$$\eta = \frac{P_{hyd}}{P_{hyd} + P_{loss}}$$

Loss decomposition:

$$P_{loss} = P_{fric} + P_{leak} + P_{visc}$$

Structural Constraints

Cavitation constraint:

$$P(\theta) \geq P_{vap}$$

Stress constraint:

$$\sigma_H \leq \sigma_{max}$$

Stability constraint:

$$\zeta \geq \zeta_{min}$$

Cam Smoothness Constraint:

$$J_{jerk} = \int_0^{2\pi} \left(\frac{d^3 s}{d\theta^3}\right)^2 d\theta$$

This enforces manufacturable and dynamically smooth cam profiles.

Full Deterministic Objective

$$J_{phys}(x) = w_1 R_\tau^2 + w_2 R_P^2 + w_3(1 - \eta) + w_4 J_{spec} + w_5 J_{jerk}$$

Gaussian Process Surrogate Model

Because evaluating $J(x)$requires expensive physics simulation approximate:

$$J(x) \sim \mathcal{GP}(m(x), k(x, x'))$$

Posterior Prediction

Mean:

$$\mu(x_*) = k_*^T (K + \sigma_n^2 I)^{-1} y$$

Variance:

$$\sigma^2(x_*) = k_{**} - k_*^T (K + \sigma_n^2 I)^{-1} k_*$$

Physics-Informed Improvement

Instead of learning full physics every iteration:

$$f(x) = J_{sim}(x) - J_{linearised}(x)$$

This ensures the GP learns only nonlinear residual behaviour, improving sample efficiency.

Bayesian Optimisation Strategy

The next design is selected via acquisition function balancing:

- exploitation (low predicted cost)
- exploration (high uncertainty)

$$x_{k+1} = \arg\min_{x}[\mu(x) - \kappa\sigma(x)]$$

Thus, the full system is a closed loop multi-scale optimisation problem as shown in the flow diagram below:

x → nonlinear periodic physics → spectral energy operator → $J(x)$ → GP surrogate → Bayesian optimisation

Modelling Limitations

While the presented model captures the dominant hydraulic and dynamic behaviour of the motor, several simplifying assumptions and modelling limitations must be acknowledged when interpreting the optimisation results.

The leakage model uses a linearised laminar-flow approximation based on Hagen–Poiseuille behaviour through annular piston clearances. While computationally efficient, this approach may underestimate losses under high pressure gradients, elevated temperatures, or transient operating conditions where turbulence, wear, surface effects, and seal dynamics become significant. Leakage is also strongly influenced by manufacturing tolerances and deformation, which are not explicitly modelled.

The fluid model assumes a spatially uniform effective bulk modulus and simplified compressibility behaviour. Although entrained air and cavitation effects are approximated through an effective compressibility term, the model does not resolve multiphase flow dynamics, vapor transport, or localized pressure-wave propagation. Consequently, cavitation behaviour and transient chamber phenomena may not be fully captured, particularly during rapid valve transitions or high-speed operation.

Valve and port flow are represented using quasi-steady orifice-flow relations with simplified opening geometry. Higher-order effects such as jet formation, vena contracta behaviour, unsteady discharge coefficients, and flow-induced oscillations are neglected. As a result, predicted chamber pressure evolution may be smoother than that of a physical system, especially during rapid commutation events.

The structural model further assumes rigid cam, piston, roller, and housing components. Elastic deformation, Hertzian contact compliance, shaft torsion, and housing deflection are neglected despite potentially significant effects at operating pressures approaching 450 bar. These phenomena may alter contact stresses, valve timing, effective piston stroke, and torque ripple behaviour.

Although a simplified thermal model is included, the simulation does not fully resolve temperature-dependent material and fluid properties. Oil viscosity, density, bulk modulus, and leakage characteristics vary substantially with temperature, while localized heating and transient thermal gradients are neglected. Consequently, long-duration efficiency predictions may differ from real operating behaviour.

Additional limitations arise from the optimisation framework itself. Restricting the cam profile to a reduced harmonic basis and smooth spline reconstruction improves manufacturability and mechanical reliability but constrains the reachable design space and may exclude unconventional local optima. Furthermore, despite the robustness of the hybrid Bayesian-gradient optimisation strategy, convergence to the global optimum cannot be guaranteed for such a highly nonlinear system.

The simulation also assumes idealised manufacturing and assembly conditions. Machining tolerances, surface roughness, misalignment, eccentricity, bearing clearances, and wear are not incorporated, despite their potential influence on leakage, vibration, efficiency, and torque ripple in practical systems.

The model is intended primarily as a comparative optimisation and preliminary design framework rather than a fully validated industrial digital twin. The results should therefore be interpreted as physically informed design guidance suitable for identifying favourable trends and candidate geometries prior to detailed finite element analysis, computational fluid dynamics, and experimental validation.

A final significant limitation concerns the translation of the mathematically optimized geometric output back into a manufacturable CAD environment. While the spline-based parameterization successfully constrained the optimiser to smooth geometric modes and eliminated high-frequency oscillatory artifacts in mathematical space, achieving a robust, automated export of the 20-point B-spline to a solid model proved technically challenging within the project timeline. This translation bottleneck manifested through three distinct iterative failure modes:

First, initial optimization runs successfully navigated away from theoretical high-frequency collapse using empirical penalty constraints. However, the automated export of these solutions yielded discrete point geometries containing severe interpolation artifacts. Although the C++ solver converged to mathematically valid B-spline control point arrays, the resulting sampled coordinate outputs exhibited jagged, non-manifold surface topologies (Figure 5). These discrete geometries lacked the continuous tangent vectors required for stable solid modelling and subsequently failed during CAD import.

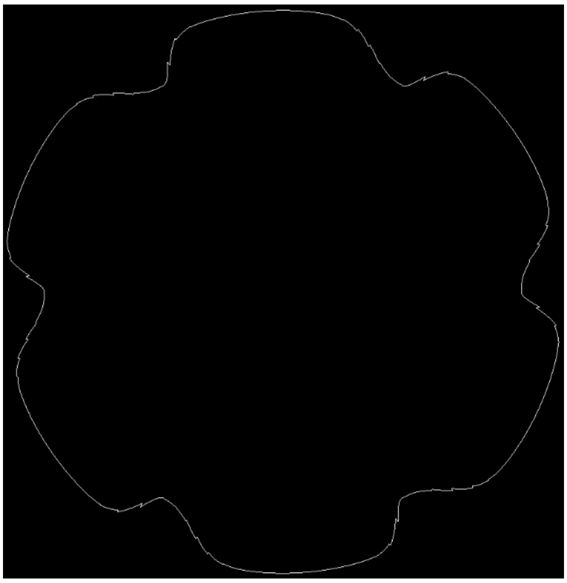

Figure 5: A DXF view of Early Optimisation run outputs.

Second, further tuning of the geometric constraint penalties was applied to force the solver to eliminate these jagged artifacts. While this successfully produced smoother control point distributions, it inadvertently drove the optimizer toward a localized 'polygonal collapse' artifact (Figure 6). In this regime, the optimizer identified that extended flat dwell regions on the cam lobes mathematically minimized chamber pressure variance. The resulting geometry closely approximated a hexagonal profile where sharp transitions at the lobe corners produced effectively infinite curvature and acceleration. While this profile satisfied the mathematical cost function, it represented a physically non-manufacturable geometry.

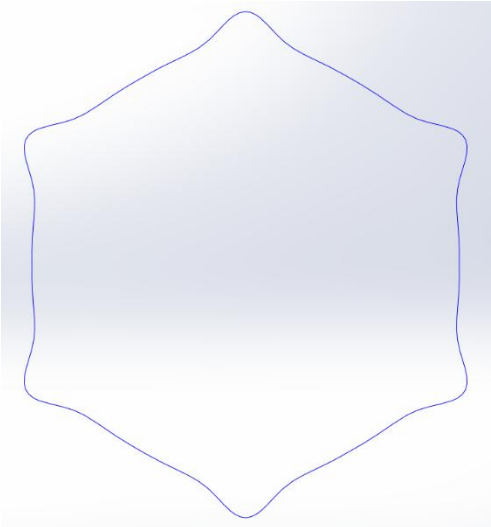

Figure 6: Later Optimization run outputs

Third, recognizing that resolving the complex periodic B-spline export algorithm and non-convex constraint boundary mapping would stall the structural validation phase, a strategic pivot was made. Consequently, the structural finite element analysis and CAD integration utilized a parametric sine-wave baseline profile generated directly within SolidWorks (Figure 7) to represent the 7-piston, 6-lobe kinematic envelope.

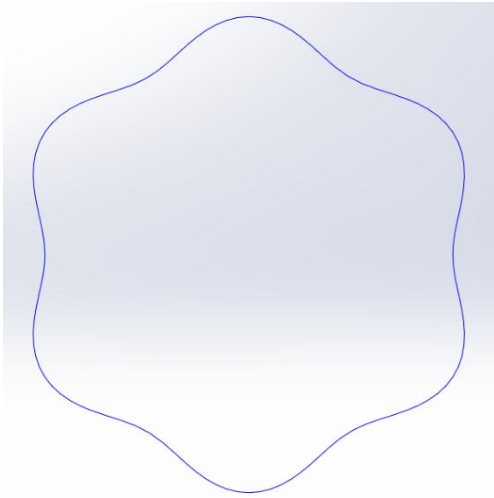

Figure 7: Final SolidWorks Parametric Curve

Because the 7/6 coprime architecture provides the dominant harmonic smoothing—reducing RMS torque ripple by >99% compared to non-coprime baselines purely through phase dispersion—this baseline profile provides a conservative but highly representative boundary condition for validating global system behaviour. It effectively isolates and validates the structural stiffness, modal frequencies, and bearing load paths of the chosen architecture. However, it is critical to note that this approach decouples the structural validation from the final micro-geometric optimizations of the lobe surface; therefore, the FEA results do not capture the highly localized contact stress variations that would arise from the final optimized lobe curvature.

Design of the Motor

The following sections now transition from the derivation of the governing mathematical and optimisation models toward their implementation within the physical architecture of the radial piston hydraulic motor. While the optimisation framework ultimately determines the final cam geometry and hydraulic timing parameters, the baseline mechanical configuration must first be selected such that the design space itself is inherently favourable from both a harmonic and physical perspective. Establishing a mechanically sensible initial architecture prior to optimisation is critically important because it reduces optimisation complexity, improves convergence behaviour, suppresses non-physical local minima, and prevents the optimiser from compensating for poor architectural choices through unrealistic geometric distortions.

In practice, optimisation alone cannot fully compensate for fundamentally poor harmonic architecture. If the piston arrangement inherently generates strong low-order excitation modes, the optimisation algorithm is forced to introduce increasingly aggressive geometric shaping in an attempt to artificially suppress the resulting torque ripple. Such behaviour frequently produces impractical curvature distributions, excessive pressure angles, unstable piston acceleration, unrealistic contact stresses, and non-manufacturable cam surfaces. Consequently, the initial selection of piston count, cam lobe count, and phase arrangement acts as a first-order harmonic filter before higher-order optimisation is even introduced.

Motor Initial Architecture and Harmonic Design Constraints

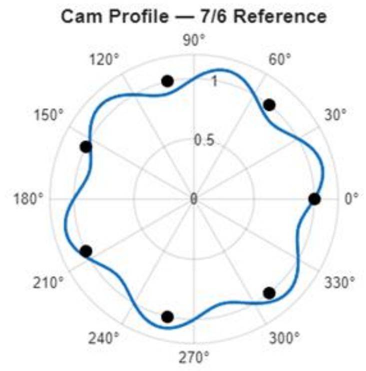

Figure 8: Cam and Piston Phasing Plot

In radial piston hydraulic motors, the dominant source of torque ripple arises from the discrete pressure application events generated as individual pistons traverse the cam profile. Unlike continuously distributed torque-producing systems, radial piston motors generate torque through a finite number of discrete hydraulic chambers distributed circumferentially around the cam surface. Each piston produces a local force contribution whose magnitude varies continuously with piston displacement, chamber pressure, contact angle, local cam curvature, and hydraulic commutation behaviour. The total output torque therefore arises from the superposition of multiple phase-shifted piston force contributions distributed throughout the rotational cycle. Figure 8 illustrates the general piston phase relationship relative to the cam geometry and demonstrates how individual piston contributions combine to form the aggregate output waveform.

Because these excitation events are periodic, the harmonic structure of the resulting torque waveform is governed primarily by the interaction between the piston count, N_p, and the cam lobe count, N_l. The relative phasing between these quantities determines whether piston contributions reinforce one another coherently or instead distribute their excitation energy throughout the rotational cycle. A critical requirement therefore emerges that the piston and lobe counts remain mutually prime:

$$\gcd(N_p, N_l) = 1$$

If a common divisor exists between the two quantities, repeated phase alignment occurs between specific pistons and specific cam lobes over successive revolutions. This repeated synchronisation produces coherent low-order harmonic reinforcement, generating large oscillatory components within the output torque waveform. Such low-frequency harmonics are particularly undesirable because they couple strongly into the mechanical inertia of the drivetrain and are only weakly attenuated by hydraulic compressibility and structural damping. The resulting behaviour manifests as increased shaft vibration, pressure pulsation, housing excitation, acoustic noise, and perceptible output torque oscillation.

By contrast, coprime piston-lobe configurations prevent repeated synchronous alignment. Each piston continuously samples unique phase positions relative to the cam geometry over the complete rotational cycle, distributing excitation energy more uniformly throughout the waveform. Rather than concentrating energy into dominant low-frequency modes, the harmonic content becomes dispersed across higher-order frequencies where oscillations are more effectively attenuated by fluid compressibility, rotating inertia, viscous damping, and structural compliance. This phase-dispersion behaviour inherently suppresses harmonic synchronisation before any further geometric optimisation is introduced.

In addition to coprimality, the relative difference between piston count and lobe count strongly influences the effective ripple frequency content. A characteristic low-order interaction frequency scales approximately with:

$$f_r \propto | N_p - N_l | \omega$$

where $\omega$is shaft rotational speed. Configurations possessing small integer separations between piston count and lobe count generally produce smoother overlap between adjacent piston contributions while simultaneously increasing the effective ripple frequency. This shift toward higher-frequency oscillation is advantageous because high-frequency disturbances possess reduced inertia coupling and are filtered more effectively by the combined hydraulic-mechanical dynamics of the motor system.

However, harmonic smoothness alone is insufficient as a design criterion. Increasing piston count indefinitely introduces significant geometric and mechanical penalties. For a fixed housing diameter, larger piston counts reduce the available bore area for each piston, decreasing displacement per chamber while simultaneously increasing leakage sensitivity, machining complexity, and manufacturing tolerance requirements. Closely packed cylinders additionally reduce the structural wall thickness between adjacent bores, increasing stress concentration and weakening the housing under peak hydraulic loading.

Conversely, reducing piston count increases the magnitude of each individual pressure impulse. Fewer pistons therefore generate larger instantaneous torque fluctuations, stronger low-order harmonic content, and increased pressure pulsation amplitude. The architecture must therefore balance firing density against achievable piston area, structural integrity, manufacturability, and volumetric performance.

The cam lobe count introduces similar trade-offs. Increasing the number of lobes raises the effective firing frequency and improves overlap smoothness but simultaneously reduces the local radius of curvature of the cam surface. Smaller curvature radii generate larger piston acceleration gradients, increased Hertzian contact stress, elevated roller loading, higher friction losses, and greater wear rates. Excessively high lobe counts may additionally introduce undercutting behaviour and machining difficulties due to aggressive local curvature transitions. Conversely, low lobe counts produce larger displacement excursions per lobe, increasing pressure pulsation magnitude and worsening low-frequency torque oscillation. While such geometries may be mechanically simpler, their harmonic behaviour becomes substantially less favourable.

To evaluate these competing effects, multiple piston-lobe architectures were investigated, including 6/6, 7/6, 8/6, 9/6, 10/6, 7/5, 7/7, and 9/7 configurations. The resulting physical torque waveforms for each architecture are presented in Figure 9, while Figure 10 additionally shows the complete least-common-multiple rotational cycle for each configuration. The full excitation pattern repeats only after the piston-lobe phase relationship returns to its initial state, occurring over a rotational interval governed by the least common multiple of N_p and N_l. These extended-cycle plots are particularly important because short-duration waveform inspection alone can conceal large-scale harmonic reinforcement behaviour. Certain configurations may appear locally smooth while still exhibiting strong spectral concentration over the full rotational period.

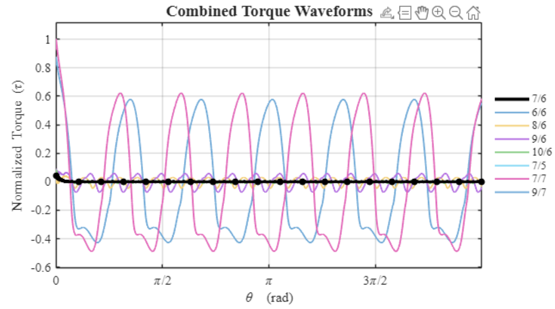

Figure 9: Normalised Torque Combined Waveforms

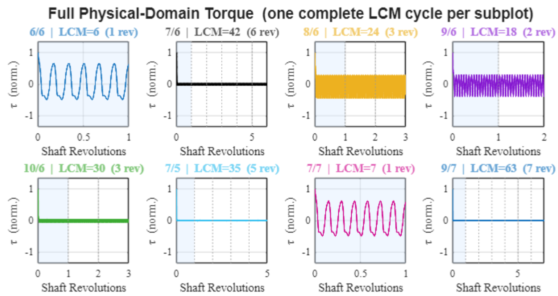

Figure 10: LCM Individual Torque Waveforms

The extended-cycle waveforms reveal several important behaviours. Non-coprime architectures such as 6/6 and 7/7 exhibit strong repeating synchronous excitation patterns, producing dominant low-order oscillations and large-amplitude torque variation. By contrast, coprime configurations distribute excitation energy more uniformly throughout the rotational cycle, suppressing dominant low-frequency modes and generating smoother aggregate torque production.

The FFT spectra corresponding to each configuration are shown in Figure 11 together with a collapsed comparison spectrum containing all architectures simultaneously in Figure 12. These figures demonstrate that favourable configurations do not merely reduce instantaneous ripple magnitude but instead redistribute harmonic energy across broader higher-order frequency regions. This spectral spreading behaviour is highly beneficial because high-frequency oscillations are attenuated far more effectively by hydraulic compliance and mechanical inertia than concentrated low-order harmonic peaks. Quantitative ripple metrics for each architecture are summarised in Table 3 on the following page.

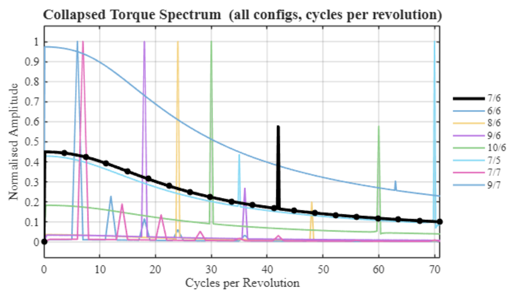

Figure 11: Individual Torque Spectral Energy Plots

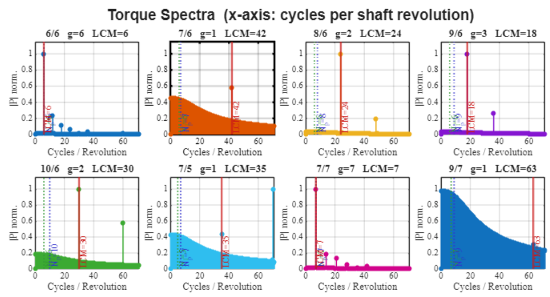

Figure 12: Normalised Combined Torque Spectra

Table 3: Quantitative Ripple Metrics

Configuration	RMS Ripple	Peak-to-Peak Ripple
6/6	0.1873	0.64089
7/6	0.00140	0.02548
8/6	0.01249	0.04213
9/6	0.02194	0.08034
10/6	0.00375	0.04658
7/5	0.00122	0.01985
7/7	0.20794	0.73488
9/7	0.00138	0.02545

However, ripple metrics alone are insufficient to determine overall architectural suitability because the cam geometry required to achieve a particular harmonic response may simultaneously introduce severe mechanical penalties. Further geometric analysis therefore investigated curvature behaviour, pressure-angle variation, contact loading, and manufacturability constraints across all candidate architectures. Figure 14 presents the cam surface curvature distributions and Figure 15 presents equivalent pressure-angle distributions for each investigated configuration together with deviation plots referenced against the final 7/6 reference architecture.

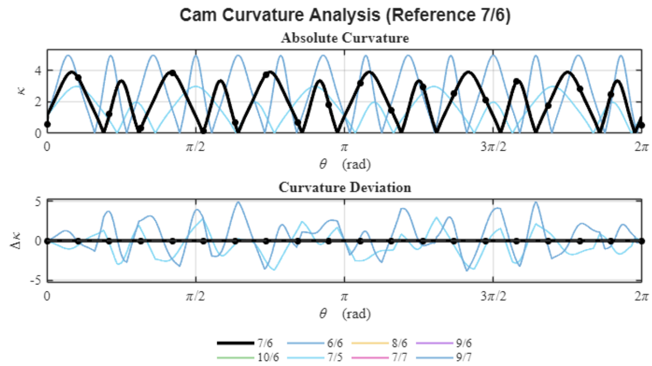

Figure 14: Cam Curvature Comparison Plots

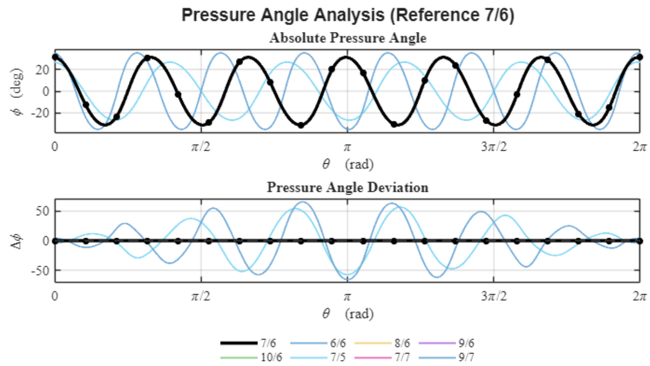

Figure 15: Cam Pressure Angle Comparison Plots

The geometric comparisons reveal that low nominal ripple magnitude alone does not necessarily correspond to favourable overall dynamic behaviour. The 7/5 architecture, despite exhibiting marginally lower ripple values, produced substantially larger displacement excursions per lobe and correspondingly higher piston acceleration gradients. This increased local contact loading, worsened pressure-angle behaviour, and generated more aggressive hydraulic chamber pressure transitions. In practice, the realised torque waveform is additionally influenced by finite chamber filling dynamics, fluid compressibility, transient pressure lag, and port timing overlap effects, further amplifying the undesirable behaviour associated with aggressive displacement profiles.

Similarly, higher piston-count configurations improved overlap smoothness but significantly reduced piston bore area, increased packaging complexity, and reduced structural wall thickness between adjacent cylinders. Architectures employing larger lobe counts additionally exhibited increasingly aggressive local curvature distributions and elevated pressure angles, leading to higher Hertzian contact stresses, increased roller loading, poorer manufacturability, and greater sensitivity to machining tolerances. Several configurations also demonstrated undesirable spectral energy concentration despite acceptable RMS ripple values, indicating that instantaneous ripple metrics alone were insufficient for evaluating overall dynamic smoothness.

The curvature and pressure-angle deviation plots further demonstrate that many alternative configurations introduced highly concentrated local curvature spikes or elevated pressure-angle regions despite achieving comparable nominal ripple metrics. By contrast, the final 7/6 architecture maintained comparatively smooth curvature transitions and moderate pressure-angle behaviour, reducing local stress concentration while preserving favourable harmonic characteristics.

When considered collectively across all evaluated criteria — including harmonic distribution, spectral energy spreading, pressure-angle behaviour, curvature smoothness, achievable piston area, packaging practicality, structural integrity, manufacturability, and dynamic stability — the seven-piston, six-lobe configuration consistently emerged as the most balanced architecture. The 7/6 configuration satisfies the coprimality condition,

$$\gcd(7,6) = 1$$

while simultaneously maintaining strong phase dispersion, favourable harmonic spreading, high effective ripple frequency, moderate pressure angles, manufacturable curvature distributions, acceptable piston bore area, practical housing dimensions, and stable dynamic behaviour. Rather than being selected arbitrarily and subsequently justified, the 7/6 architecture emerged naturally from the combined harmonic, geometric, hydraulic, and mechanical analysis as the most physically balanced solution for the intended operating regime.

Several additional geometric and physical constraints were also required to ensure that all candidate geometries remained physically realisable prior to optimisation. Firstly, the minimum cam curvature radius had to exceed the roller radius plus an allowable stress margin in order to prevent undercutting and excessive local contact stress. Excessively sharp local curvature rapidly increases Hertzian contact pressure, accelerating wear, surface fatigue, lubrication breakdown, and potential roller instability.

Secondly, piston spacing had to maintain sufficient wall thickness between adjacent cylinders to preserve structural integrity under peak hydraulic pressure loading. Excessive piston density may improve harmonic overlap while simultaneously weakening the housing structure and increasing manufacturing complexity. Thirdly, piston stroke limits needed to remain compatible with seal travel capability, port timing geometry, and practical housing dimensions. Excessive stroke lengths increase seal wear, worsen dynamic loading, increase piston side loading, and complicate hydraulic port timing behaviour.

Consequently, the optimisation process operated within constrained bounds defined not only by performance objectives, but also by contact stress limitations, cavitation avoidance, volumetric efficiency requirements, leakage constraints, manufacturable cam geometry, achievable machining tolerances, bearing load capacity, structural rigidity, piston acceleration limits, and overall dynamic stability requirements.

The combined hydraulic-mechanical behaviour of the motor may additionally be interpreted using the mass-spring-damper analogy illustrated in Figure 16. In this representation, rotating inertia acts as the mass element, fluid compressibility behaves as an effective spring, and viscous hydraulic losses provide damping. This analogy provides physical insight into why higher-frequency ripple components are preferentially attenuated while low-frequency oscillations propagate more effectively into the drivetrain, further explaining why redistributing harmonic energy toward higher frequencies is often more beneficial than attempting to eliminate ripple magnitude entirely.

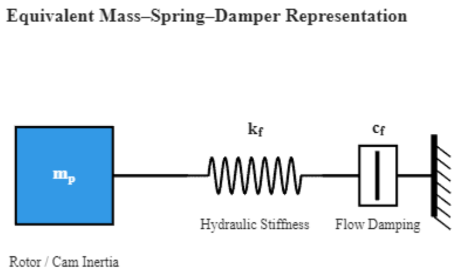

Figure 16: Mass-Spring-Damper Analogy

Cam Profile Representation and Basis Function Selection

Because the optimiser operates directly on the cam geometry, the mathematical basis used to represent the cam profile strongly influences not only optimisation dimensionality, but also optimisation stability, physical realism, and the susceptibility of the optimiser to non-physical solutions.

Several candidate representations were investigated, including Fourier series expansions, global polynomial basis functions, and periodic B-spline parameterisations. Figure 17 presents a direct comparison between these basis representations together with their resulting curvature distributions, pressure-angle behaviour, and spectral energy content.

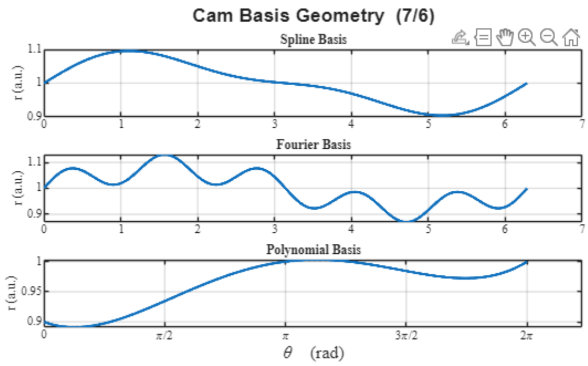

Figure 17: Cam Basis Geometry Comparison

Initial investigations using Fourier basis representations revealed several significant limitations despite their apparent suitability for periodic geometry. Fourier expansions naturally provide direct access to harmonic manipulation and can efficiently represent smooth periodic functions. However, in practice they also permit the optimiser to artificially suppress ripple through the injection of extremely high-order harmonic oscillations.

This behaviour produces a major optimisation pathology. The optimiser effectively "cheats" by introducing narrow high-frequency geometric oscillations which mathematically reduce simulated torque ripple while simultaneously generating unrealistic curvature spikes, unstable piston acceleration, excessive contact stress, impractical pressure angles, and non-manufacturable surface geometry.

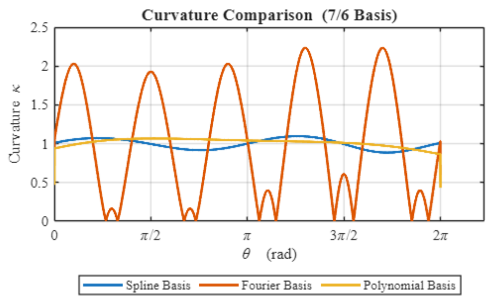

Figure 18: Cam Basis Functions Curvature

The resulting geometries often appear favourable numerically while being physically impossible to manufacture or dynamically unstable during operation. Figures 18, 19, and 20 demonstrate this behaviour directly through the comparative curvature, pressure angle and spectral energy plots respectively, which exhibit strong high-frequency energy concentration and local curvature spikes absent in the spline representation.

Polynomial basis functions exhibited similarly problematic behaviour. Because polynomial coefficients influence the entire domain globally, small parameter adjustments frequently generated large unintended geometric distortions elsewhere along the profile. Higher-order polynomials additionally suffered from oscillatory instability, poor periodic continuity behaviour, and excessive endpoint sensitivity.

For these reasons, the final optimisation framework adopts a reduced-order periodic B-spline representation consisting of:

$$N_{\mathrm{ctrl}} = 20$$

control points.

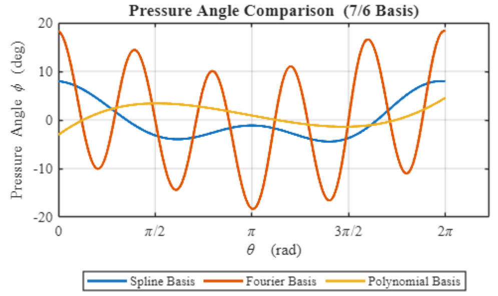

Figure 19: Cam Basis Functions Pressure Angle

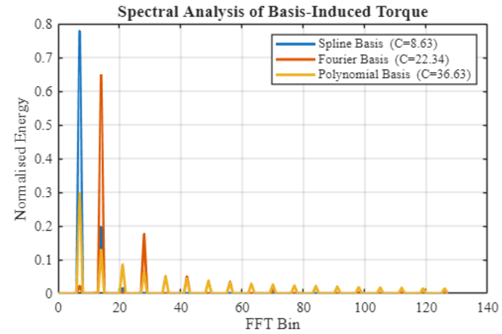

Figure 20: Cam Basis Spectral Analysis

The cam profile is parameterised as:

$$C(\theta) = \sum_{i=0}^{N_{\mathrm{ctrl}}-1} N_{i,p}(\theta) P_i$$

where $N_{i,p}(\theta)$are periodic B-spline basis functions of degree p, and $P_i$are the radial control points defining the cam geometry.

The spline representation provides several substantial advantages over both Fourier and polynomial alternatives.

Firstly, periodic B-splines inherently satisfy continuity conditions across the full rotational domain. Because the initial and final control points are identified periodically,

$$P_0 = P_{N_{\mathrm{ctrl}}}$$

the resulting cam geometry remains continuous in position, slope, and curvature across the complete rotational cycle. This continuity is essential for stable piston acceleration behaviour and manufacturable toolpath generation.

Secondly, B-splines provide strong local geometric control. Adjusting a single control point affects only a limited neighbourhood of the curve rather than globally distorting the entire profile. This locality dramatically improves optimiser stability and prevents unintended geometric coupling between unrelated regions of the cam surface.

Thirdly, spline parameterisations naturally suppress unrealistic high-frequency oscillations. Unlike Fourier representations, spline bases cannot easily generate arbitrarily sharp local oscillations without simultaneously violating curvature constraints and smoothness penalties. This behaviour significantly reduces the optimiser's ability to exploit non-physical harmonic artefacts.

Finally, the spline representation dramatically reduces optimisation dimensionality while preserving geometric fidelity. Rather than optimising thousands of geometric coordinates directly, the optimiser operates only on the dominant geometric modes that meaningfully influence torque production and ripple behaviour. The final high-resolution geometry is subsequently reconstructed from the spline representation for simulation and CAD generation.

To prevent non-physical geometries, all spline control points are constrained within feasible radial bounds:

$$r_{\min} \leq P_i \leq r_{\max}$$

thereby preventing self-intersection, negative lift regions, and insufficient wall thickness.

A smoothness regularisation term is additionally introduced:

$$P_{\text{smooth}} = \sum_{i=0}^{N_{\text{ctrl}}-1} (P_{i+1} - 2P_i + P_{i-1})^2$$

This penalty acts similarly to a geometric low-pass filter by discouraging excessive local curvature oscillation and suppressing unrealistic high-frequency geometric behaviour.

Implementation of the Optimiser Loop

The optimisation framework was developed to solve a strongly coupled multi-physics design problem in which cam geometry, piston kinematics, valve timing, fluid compressibility, leakage behaviour, cavitation response, and harmonic torque production are all highly interdependent.

The resulting objective landscape is extremely nonlinear and strongly non-convex. Numerous local minima exist due to harmonic interactions between pistons, lobes, hydraulic timing events, and fluid compressibility effects. Conventional analytical optimisation approaches are therefore insufficient, particularly because local gradients alone provide poor global search capability within such a highly multimodal design space.

Consequently, the optimisation problem was formulated as a constrained hybrid global-local search architecture operating on the reduced spline parameterisation of the cam geometry.

The optimiser simultaneously varies:

- spline control point locations,
- valve phase shift,
- valve opening duration,
- and valve overlap width.

The complete design vector is therefore expressed as:

$$x = [P_0, P_1, \dots, P_{N_{\text{ctrl}}-1}, \phi_v, w_v, o_v]$$

These valve timing parameters strongly influence chamber pressurisation and decompression timing, thereby coupling hydraulic dynamics directly into the torque ripple response. Optimising cam geometry independently of valve timing would therefore produce fundamentally suboptimal solutions due to phase mismatch between piston displacement and chamber pressure evolution.

The complete objective function is formulated as a weighted multi-objective metric:

$$J = w_1 R_T + w_2 P_{\text{loss}} + w_3 C + w_4 (1 - \eta_v) + P_{\text{constraints}}$$

where:

R_T is torque ripple magnitude,

P_{loss} represents hydraulic and leakage losses,

C is a cavitation penalty term,

η_v is volumetric efficiency,

and $P_{\text{constraints}}$ contains feasibility and smoothness penalties.

The inclusion of penalty terms is essential because many mathematically optimal solutions are physically unrealizable. Without regularisation, the optimiser naturally attempts to generate sharp local geometric distortions which artificially suppress simulated ripple while producing unstable piston acceleration and impractical surface geometry.

Because direct evaluation of the full hydraulic simulation is computationally expensive, the optimisation architecture employs a hybrid Bayesian-global and local-gradient refinement strategy. Figure 21 presents the complete Gaussian Process optimiser flow diagram including surrogate construction, acquisition evaluation, simulation refinement, constraint projection, and convergence stages.

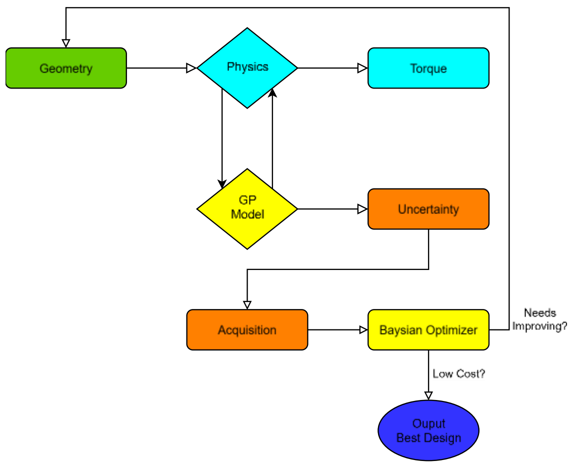

Figure 21: GP and Bayesian Optimizer Flow Chart

A Gaussian Process surrogate model approximates the objective landscape using the squared exponential covariance kernel:

$$k(x_i, x_j) = \sigma^2 \exp\left(-\frac{\parallel x_i - x_j \parallel^2}{2l^2}\right)$$

where l is the characteristic length scale and σ^2 is the signal variance.

The Bayesian acquisition strategy employs a lower-confidence-bound formulation:

$$A(x) = \mu(x) - \kappa\sigma(x)$$

where $\mu(x)$ is the predicted objective value, $\sigma(x)$ is predictive uncertainty, and κ controls the exploration-exploitation balance.

This acquisition strategy intentionally samples regions possessing either low predicted cost or high uncertainty, thereby preventing premature convergence into poor local minima.

Candidate solutions identified by the Bayesian exploration stage are subsequently refined using local numerical gradient optimisation computed directly from the full hydraulic simulation model. This hybrid architecture combines the global exploration capability of Bayesian optimisation with the rapid local convergence behaviour of gradient-based refinement.

Finally, all candidate solutions are continuously projected back into physically feasible regions during each optimisation iteration. These constraints include:

- curvature limits,
- pressure angle bounds,
- valve timing constraints,
- overlap limits,
- smoothness requirements,
- periodic continuity,
- manufacturable geometry conditions,
- and cavitation stability bounds.

Embedding these constraints directly within the optimisation framework ensures that the search process remains restricted to physically manufacturable and dynamically stable solutions throughout the optimisation procedure rather than relying on post-processing rejection criteria after optimisation completion.

Simulation Results and Discussion

Following the development of the mathematical model, optimisation framework, and preliminary architecture selection, the final motor configuration was evaluated using the full C++ simulation environment. This stage represents the primary validation of the optimised hydraulic, geometric, and harmonic design prior to structural finite element analysis and experimental verification.

The purpose of the simulation stage is not to further refine the governing equations, but to evaluate the emergent physical behaviour of the completed seven-piston, six-lobe geometry under nominal operating conditions and the optimization of the cam profile to minimize undesirable traits. Particular emphasis is placed on system-level harmonic redistribution, dynamic stability, hydraulic continuity, cavitation suppression, energetic efficiency, and numerical robustness.

All results are interpreted within a coupled multi-physics framework in which cam geometry, piston kinematics, chamber pressure evolution, and valve timing jointly determine system output behaviour. Improvements observed in individual signals are therefore not treated in isolation but as manifestations of a shared reduction in low-order excitation modes across the system.

Optimiser Convergence and Model Stability

Figure 22 presents the optimisation convergence history alongside the evolution of Gaussian Process predictive uncertainty throughout the optimisation process.

The convergence behaviour demonstrates a characteristic transition from high-variance exploratory search to stabilised local exploitation. In the initial stages, the objective function exhibits large fluctuations due to sparse sampling of the design space. This behaviour is expected, as the Gaussian Process surrogate model initially possesses limited information regarding the highly nonlinear relationship between cam geometry, valve timing, and hydraulic response.

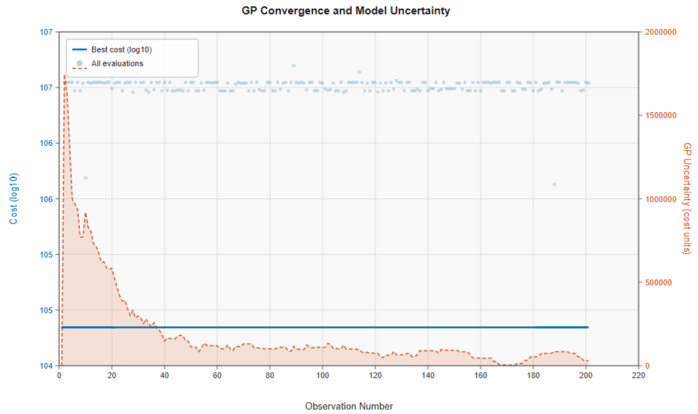

Figure 22: GP Convergence and Uncertainty

During this phase, the Bayesian acquisition strategy prioritises regions of high uncertainty, resulting in candidate solutions that explore diverse geometric and timing configurations. Consequently, early objective evaluations exhibit significant variation, reflecting the sensitivity of torque ripple and pressure behaviour to small geometric perturbations.

As the optimisation progresses, the surrogate model incrementally refines its approximation of the objective landscape. This results in a gradual reduction in both objective magnitude and predictive uncertainty, particularly in the vicinity of high-performing solutions. The convergence trajectory ultimately stabilises, indicating that the optimiser has identified a consistent region of favourable geometric and hydraulic configurations.

A key feature of the observed convergence behaviour is the absence of oscillatory divergence or instability in the final stages of optimisation. This is directly attributable to the spline-based cam parameterisation, which enforces local geometric continuity and suppresses high-frequency oscillatory artefacts that were previously observed in Fourier-based representations.

Earlier Fourier-based implementations frequently produced artificially low objective values by exploiting high-frequency geometric oscillations. While numerically favourable, these solutions introduced non-physical behaviour including:

- unrealistic curvature spikes,
- unstable piston acceleration profiles,
- excessive pressure angle variation,
- and poor manufacturability.

In contrast, the spline-based representation constrains the solution space to smooth, physically meaningful geometries, resulting in a more stable and interpretable optimisation trajectory. The progressive reduction in Gaussian Process uncertainty further indicates that the surrogate model is converging toward a consistent local topology in the design space, rather than overfitting isolated sampling artefacts. This provides additional confidence that the final solution corresponds to a physically meaningful optimum rather than a numerical anomaly.

System-Level Dynamic Response (Flow, Torque, and Power)

The flow, torque, and power outputs of the system arise from a shared underlying mechanism governed by piston displacement, chamber pressurisation, and valve timing. As a result, these outputs are strongly coupled and exhibit correlated harmonic structure throughout the rotational cycle.

Rather than treating each output independently, the system response is interpreted as a unified multi-domain manifestation of the same hydraulic-mechanical interaction.

Flow Behaviour

The simulated flow waveform (Figure 23) demonstrates smooth and continuous fluid delivery throughout the complete rotational cycle. Chamber transitions between intake and discharge phases occur without abrupt discontinuities, indicating effective alignment between piston displacement and valve timing.

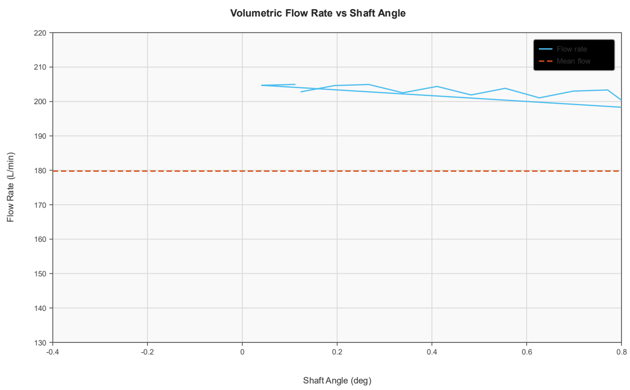

Figure 23: Optimiser Results for Volumetric Flow Rate

In earlier non-optimised configurations, flow behaviour exhibited sharp transient spikes during commutation events. These were primarily caused by mismatches between piston velocity profiles and port opening phases, resulting in sudden fluid acceleration and pressure equalisation events. In the optimised configuration, these effects are significantly reduced. Flow transitions occur more gradually, indicating improved overlap between adjacent chamber contributions. Although residual oscillations remain, they are predominantly shifted toward higher harmonic frequencies, where they are more effectively attenuated by fluid compressibility and viscous damping mechanisms.

Torque Behaviour

The torque waveform (Figure 24) demonstrates a substantial reduction in low-order oscillatory behaviour compared to baseline architectures. Instead of exhibiting periodic large-amplitude torque pulses, the output torque remains comparatively smooth across the rotational cycle.

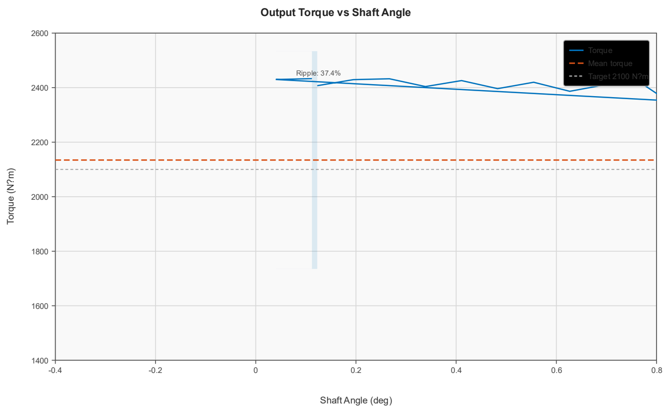

Figure 24: Optimiser Results for Output Torque and Ripple

This improvement is primarily attributed to the seven-piston, six-lobe architecture, which enforces coprime phase relationships between piston excitation events and cam lobe interactions. This prevents repeated synchronous reinforcement of low-frequency harmonic modes.

As a result, piston force contributions are more uniformly distributed across the rotational cycle, reducing coherent low-order torque accumulation. The remaining oscillatory content is primarily distributed across higher harmonic frequencies, which couple less effectively into drivetrain inertia and are more readily damped by hydraulic and structural compliance.

The FFT analysis confirms that harmonic energy is no longer concentrated in a small number of dominant peaks but is instead distributed across a broader spectral range.

Power Behaviour

The instantaneous power output (Figure 25) closely follows the torque waveform due to constant shaft rotational speed. However, power analysis provides additional insight into the continuity of energy transfer within the system. The optimised configuration exhibits smooth and continuous power delivery with no significant transient spikes. This indicates that energy conversion between hydraulic and mechanical domains occurs in a more uniform manner throughout the cycle.

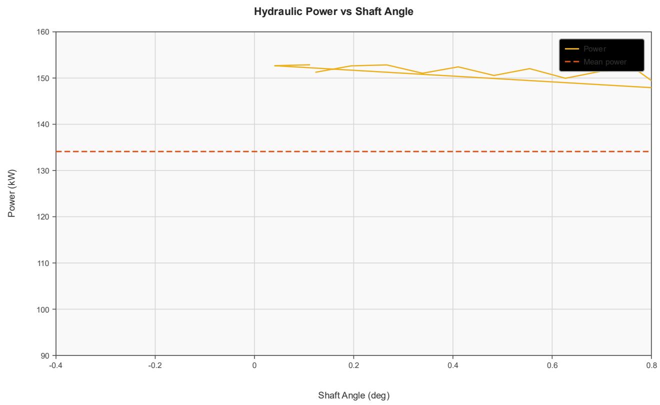

Figure 25: Optimiser Results for Hydraulic Power

Earlier configurations exhibited sharper power fluctuations associated with abrupt chamber commutation and pressure redistribution events. These fluctuations contribute to increased vibration, acoustic noise, and fatigue loading. In the optimised system, improved phase alignment between piston motion and chamber pressure evolution reduces these discontinuities, resulting in a more stable energetic output profile.

Fluid State Evolution and Stability

The chamber pressure evolution plays a central role in determining system behaviour, as it directly governs piston force generation, torque output, and flow characteristics.

In the optimised configuration, pressure transitions remain smooth and continuous throughout the rotational cycle. This indicates improved synchronisation between piston displacement, valve timing, and chamber filling dynamics.

Earlier designs exhibited abrupt pressure collapses during valve transition events due to poor phase alignment between piston motion and port exposure. These events resulted in transient low-pressure regions and increased susceptibility to cavitation.

In contrast, the optimised geometry significantly reduces the magnitude and frequency of such events. Pressure evolution is characterised by smoother gradients and improved continuity across commutation boundaries. Cavitation risk is evaluated using the condition:

$$P < P_v$$

The optimised system exhibits substantially fewer occurrences of sub-vapour-pressure conditions. This reduction is primarily attributed to improved chamber filling continuity and reduced transient pressure lag during valve transitions. Because cavitation is strongly associated with material erosion, acoustic emission, and efficiency loss, its reduction represents a significant improvement in both performance and durability.

Energetic Performance and Loss Mechanisms

Energy conversion within the hydraulic motor is governed by the balance between useful mechanical output and losses arising from leakage, viscous dissipation, and transient throttling effects.

In the optimised configuration, improved pressure continuity and reduced low-frequency oscillation contribute to a reduction in transient loss mechanisms. In particular, smoother chamber transitions reduce throttling losses associated with rapid pressure equalisation events.

Volumetric efficiency remains stable under the simulated operating conditions, despite the inclusion of realistic leakage and compressibility effects. This indicates that the optimisation process successfully improved energetic consistency without compromising hydraulic sealing behaviour.

Hydraulic losses remain dominated by leakage flow, viscous dissipation, and transient pressure redistribution. However, the magnitude of these losses is reduced relative to baseline configurations due to improved flow and pressure smoothness.

System-Level Performance Synthesis

When considered collectively, the simulation results demonstrate a consistent system-level improvement in dynamic stability across all physical domains.

Figure 26 shows the final simulation results. Rather than eliminating ripple magnitude entirely, the optimisation process redistributes harmonic energy away from dominant low-frequency modes toward higher-frequency components. This redistribution is significant because higher-frequency oscillations are more effectively attenuated by fluid compressibility, viscous damping, and structural inertia.

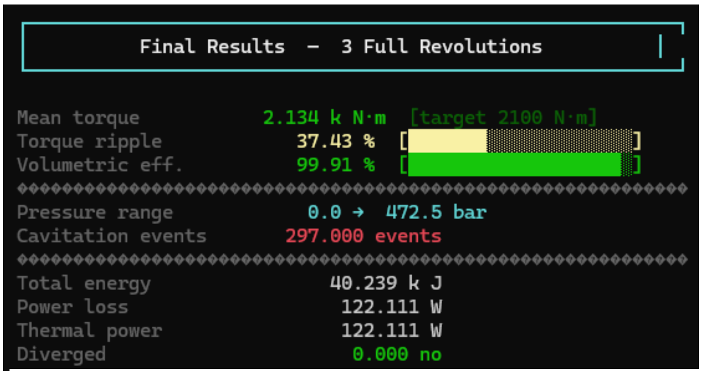

Figure 26: Final Simulation Results

This mechanism results in three key system-level outcomes:

- reduced low-order torque ripple,
- improved pressure stability,
- and smoother flow and power delivery.

Importantly, these improvements are not isolated but emerge from a unified coupling between cam geometry, piston kinematics, valve timing, and hydraulic response. The consistency of improvements across all simulated outputs confirms that the optimisation framework successfully aligned multi-domain system behaviour rather than tuning individual performance metrics independently.

Final Simulation Assessment

Overall, the simulation results validate that the optimised seven-piston, six-lobe architecture achieves stable and physically consistent behaviour under nominal operating conditions.

The system demonstrates:

- stable convergence behaviour during optimisation,
- smooth and continuous flow characteristics,
- reduced low-frequency torque ripple,
- distributed harmonic spectral energy,
- stable chamber pressure evolution,
- reduced cavitation susceptibility,
- and consistent energetic performance.

Crucially, these results indicate that the final geometry is not only numerically optimal within the simulation framework, but also dynamically realistic and physically plausible when interpreted through coupled hydraulic-mechanical principles.

The simulation stage therefore provides strong validation of the spline-based optimisation approach and the coprime piston-lobe architecture, demonstrating their combined effectiveness in producing a hydraulically smooth and mechanically stable radial piston motor design suitable for subsequent structural verification and experimental implementation.

Structural Analysis and Finite Element Validation

Following the completion of the optimisation and system-level simulation stages, the final seven-piston, six-lobe motor configuration was subjected to detailed structural and finite element analysis. While the optimisation framework primarily targeted harmonic performance, torque ripple reduction, and hydraulic efficiency, the structural analysis stage serves to verify that the resulting geometry remains mechanically feasible under realistic loading conditions.

Because the motor operates under high-pressure cyclic hydraulic loading, the structural response of the system plays a critical role in determining fatigue life, contact durability, sealing integrity, and long-term dimensional stability. In particular, the coupled interaction between hydraulic pressure, piston reaction forces, cam contact loading, and bearing support reactions introduces a complex multi-axial stress state that must be evaluated across both local and global scales.

The finite element studies therefore focus on identifying:

- global deformation behaviour,
- local contact stress concentrations,
- fatigue performance under cyclic loading,
- modal response characteristics,
- and structural integrity of key load-bearing subsystems.

CAD Model and System Architecture

A full parametric CAD assembly was developed to represent the complete motor geometry, incorporating all major hydraulic, mechanical, and structural subsystems. The model was constructed directly from the optimised cam spline representation and subsequently converted into a manufacturable 3D geometry suitable for finite element discretisation and engineering drawing generation.

The assembly includes the following primary components:

- cam ring,
- radial pistons,
- piston rollers,
- housing structure,
- shaft interface,
- bearing supports,
- valve plate geometry,
- and sealing interfaces.

The overall layout preserves the seven-piston, six-lobe architecture selected during the harmonic optimisation stage. Special care was taken to maintain uniform angular spacing and phase distribution of pistons to ensure that the structural model remains consistent with the previously validated dynamic model.

Figure 27 illustrates the full motor assembly, including sectional views showing the internal piston-cam interactions and hydraulic chamber arrangement.

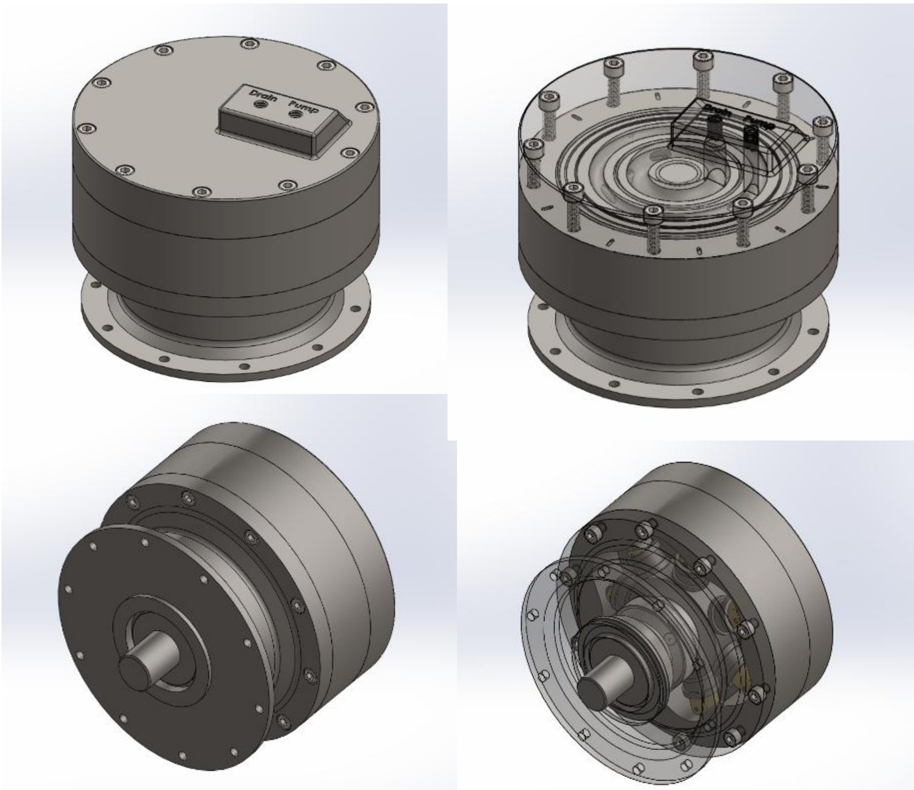

Figure 27: Motor Assembly Views

Cam Ring Structural Design

The cam ring represents one of the most structurally critical components of the system, as it directly converts hydraulic pressure into mechanical torque through repeated rolling contact with the piston rollers.

The final cam geometry was generated from the optimised spline representation and subsequently smoothed and reconstructed into a continuous manufacturable surface. Several structural constraints governed the final design:

- minimum curvature radius limits,
- pressure angle constraints,
- contact stability requirements,
- machining feasibility,
- and local stiffness considerations.

Fillet transitions were introduced throughout the cam profile to reduce stress concentrations and improve fatigue resistance under repeated cyclic loading.

The final cam ring thickness was selected to ensure that elastic deformation remains sufficiently small such that piston kinematics are not significantly altered under peak hydraulic loading. This is essential because even minor geometric distortion of the cam profile can introduce measurable deviations in torque ripple and harmonic behaviour.

Piston Structural Design

The pistons operate as pressure-loaded translating elements that transmit hydraulic force to the cam via roller interfaces. As such, they are subjected to combined loading conditions including:

- internal hydraulic pressure,
- contact forces at the roller interface,
- inertial effects due to reciprocating motion,
- and secondary bending stresses.

The piston geometry was therefore designed to balance structural strength, manufacturability, and sealing performance.

Key design considerations include:

- sufficient cross-sectional area for pressure containment,
- adequate wall thickness to resist hoop stress,
- smooth internal transitions to reduce stress concentration,
- and robust roller support integration.

Chamfers and radiused transitions were incorporated into all critical internal features to reduce stress concentration factors and improve fatigue resistance under cyclic operation. Figure 28 illustrates the piston and cam geometry coupling.

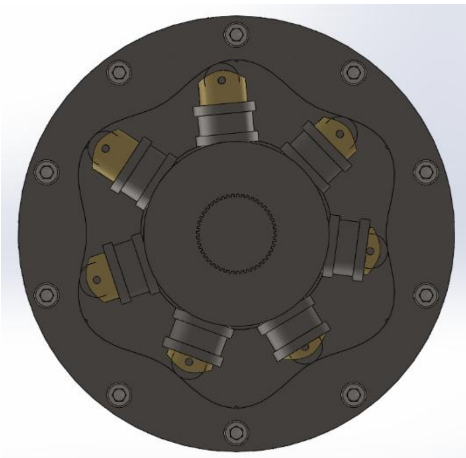

Figure 28: Cam and Piston Coupling

Rotor Structural Design

The housing serves as the primary pressure containment structure and provides the mechanical foundation for the entire motor assembly, including piston bores, bearing supports, and sealing interfaces.

It is subjected to:

- internal hydraulic pressure loading,
- reaction forces transmitted through pistons and cam contact,
- bearing-induced shaft loads,
- and assembly preload conditions.

The housing design therefore prioritises global stiffness and deformation control, particularly in regions associated with:

- cylinder bore alignment,
- bearing seat stability,
- and sealing surface flatness.

Maintaining bore circularity under load is essential, as even small deviations can introduce uneven piston loading, increased leakage, and degraded harmonic performance. Figure 29 shows the housing geometry with an internal sectional view.

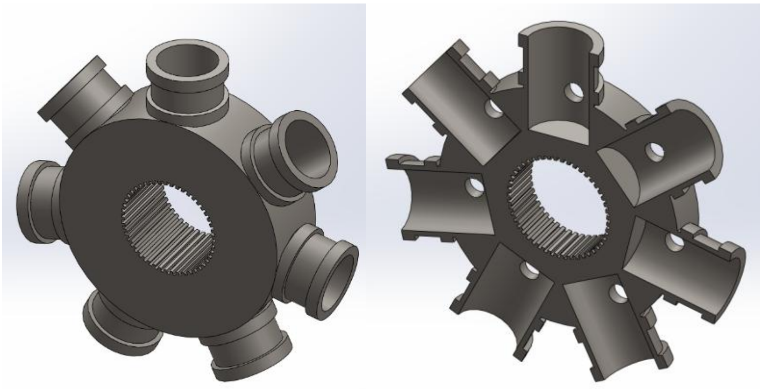

Figure 29: Rotor Geometry and Sectional View

Finite Element Analysis Overview

A series of nonlinear finite element analyses were conducted to evaluate the structural response of the motor under peak operating conditions. These simulations include:

- nonlinear contact stress analysis,
- fatigue life estimation,
- modal (vibration) analysis,
- cam ring deformation analysis,
- and bearing support stress evaluation.

Each analysis isolates a specific subsystem in order to identify critical stress regions and evaluate overall structural feasibility under realistic loading conditions.

Contact Stress Analysis (Cam–Piston Interface)

A nonlinear contact analysis (Figure 30) was performed to evaluate the rolling interaction between piston rollers and the cam surface under peak hydraulic loading conditions. The contact problem is inherently nonlinear due to load-dependent contact area variation and local deformation effects. The simulation predicted a maximum stress magnitude of approximately:

$\sigma_{max} \approx 4 \times 108\ Pa$ within the piston wall structure.

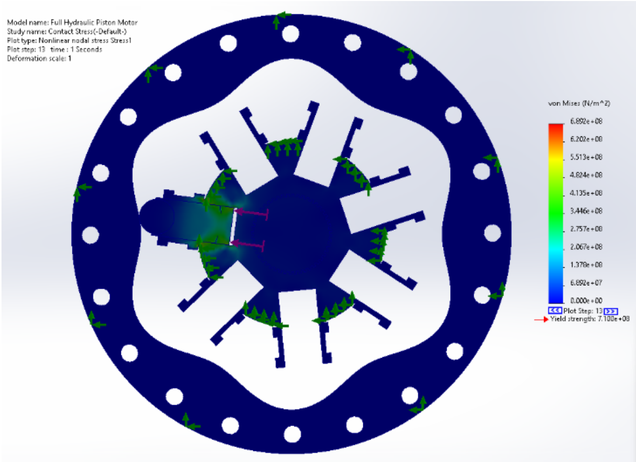

Figure 30: Contact Stress FEA (Stress)

Interestingly, the highest stresses were not concentrated directly at the contact interface but instead appeared within adjacent piston wall regions. While numerical effects such as mesh coarseness in the contact region, penalty-based contact stiffness assumptions, simplified boundary constraints, and limited local geometric refinement at the interface may contribute to this distribution, a physical bending-stress mechanism is highly probable. In a radially loaded piston with an offset roller interface, the normal contact force generates a bending moment across the piston cross-section. If the piston length-to-diameter ratio and roller offset are not perfectly balanced, this bending moment can drive peak wall stresses above the pure surface contact stress.

As a result, the reported stress field should be interpreted as a first-order approximation of the contact behaviour that captures global load redistribution effects, rather than a purely localized Hertzian stress solution.

The analysis also predicted:

- $\sigma_{max} \approx 3 \times 10^{-2}\ mm$
- $\epsilon_{max} \approx 3 \times 10^{-3}$

These values indicate that overall deformation remains small relative to characteristic geometric dimensions, suggesting that no global structural instability is expected under nominal operating conditions. However, the wall stress concentration warrants further investigation using a refined 3D sub-model to explicitly separate bending-induced principal stresses from localized Hertzian contact stresses before finalizing the piston geometry.

Fatigue Analysis

A fatigue analysis (Figure 31) was conducted to evaluate long-term structural durability under cyclic loading conditions representative of continuous motor operation.

The results indicate that the critical structural components are capable of withstanding more than 10^6 loading cycles without predicted fatigue failure under nominal operating conditions.

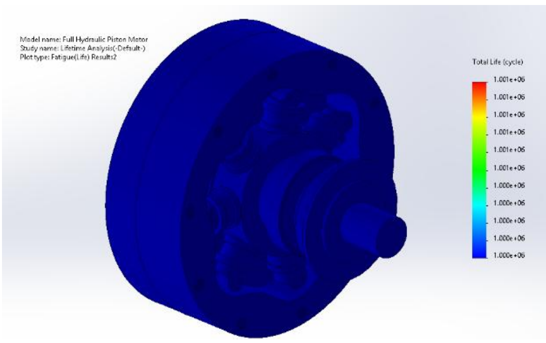

Figure 31: Fatigue FEA (Lifetime)

This favourable fatigue performance is primarily attributed to:

- smooth geometric transitions,
- high strength components,
- reduced low-frequency torque ripple due to harmonic optimisation,
- moderated pressure angle variation,
- and controlled cam curvature distribution.

However, fatigue predictions remain dependent on material assumptions and idealised loading conditions. Real-world effects such as surface roughness, lubrication variation, manufacturing tolerances, and transient pressure spikes may reduce actual fatigue life relative to simulation predictions.

Modal Analysis

A modal analysis (Figure 32) was performed to determine the natural frequencies of the assembled structure and assess the potential for resonance under operational excitation.

The first significant structural mode was identified at approximately:

$$f_n \approx 1073\,Hz$$

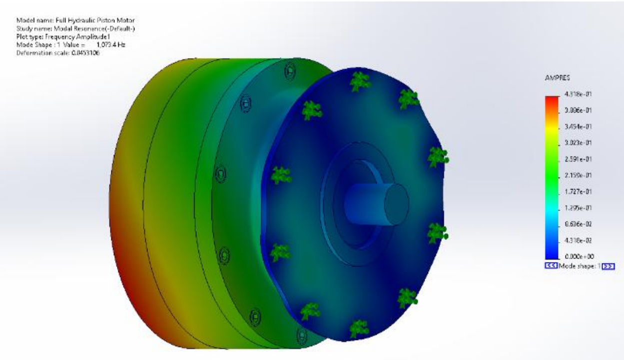

Figure 32: Modal Analysis FEA (AMPRES)

The dominant excitation frequency of the motor at 600 RPM $(\approx\ 10\,Hz)$, including primary harmonic components associated with piston-lobe interactions, remains well below the first structural mode.

Even when considering higher-order harmonic content, the excitation spectrum remains sufficiently separated from the primary structural resonance range. This separation reduces the risk of resonance amplification effects such as:

- increased vibration amplitude,
- elevated stress cycling,
- acoustic noise generation,
- and accelerated fatigue accumulation.

The modal results therefore indicate that the structure possesses adequate dynamic stiffness for the intended operating regime.

Cam Ring Loading Analysis

A dedicated loading analysis (Figure 33) was performed on the cam ring under peak pressure loading conditions to evaluate its structural rigidity and influence on piston kinematics.

The simulation results indicate:

maximum stress $\sigma_{max} \approx 3 \times 10^7 Pa$
maximum displacement $s_{max} \approx 1.13 \times 10^{-3} mm \ (1.13\ microns)$
maximum strain $\epsilon_{max} \approx 5 \times 10^{-5}$

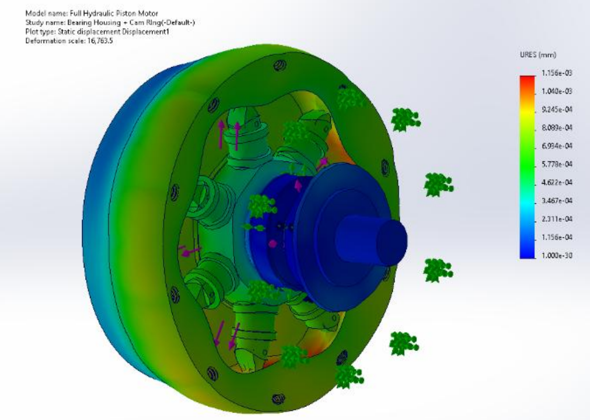

Figure 33: Cam Ring Loading FEA (Displacement, mm)

These values confirm that the cam ring remains highly rigid under operational loading conditions. Elastic deformation is sufficiently small that it does not meaningfully alter piston motion or disrupt the harmonic characteristics established during the optimisation phase.

This result is particularly important, as cam deformation would directly affect displacement profiles and introduce unwanted deviations in torque ripple behaviour.

Bearing Support Stress Analysis

A structural analysis of the bearing support system (Figure 34) was conducted to evaluate shaft loading transmission and local structural deformation.

The simulation results indicate:

maximum stress $\sigma_{max} \approx 1 \times 10^8 Pa$
maximum deflection $s_{max} \approx 1.8 \times 10^{-2}\ mm$
maximum strain $\epsilon_{max} \approx 3.6 \times 10^{-4}$

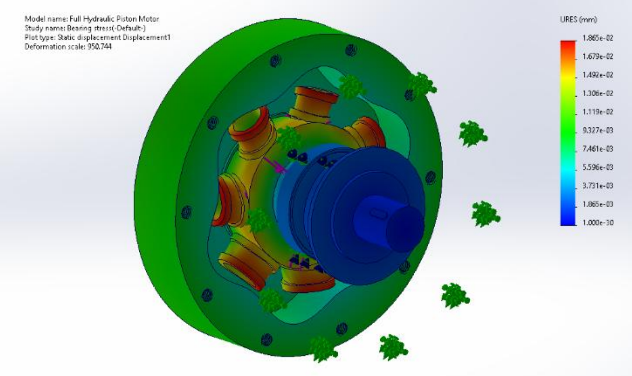

Figure 34: Bearing Stress FEA (Displacement, mm)

These results demonstrate that the bearing support structure maintains adequate stiffness under combined radial and axial loading conditions. Deformation remains small enough to preserve shaft alignment and prevent significant distortion of piston-cam contact geometry.

Discussion of Structural Results

The combined finite element analyses indicate that the selected seven-piston, six-lobe architecture is structurally feasible under the assumed operating conditions.

Across all subsystems, the results demonstrate:

- low global deformation,
- acceptable local stress magnitudes,
- stable fatigue performance under cyclic loading,
- and sufficient separation between excitation and structural natural frequencies.

Importantly, the structural behaviour is consistent with the assumptions made during the optimisation stage. In particular, the reduced pressure angle variation and smooth cam curvature produced by the spline-based optimisation framework contribute directly to reduced stress concentration and improved load distribution.

Several limitations were identified during the analysis. The most significant relates to the contact stress model, where the apparent reduction in interface stress concentration suggests that additional refinement is required. A higher-fidelity model incorporating:

- refined mesh density,
- advanced contact formulations,
- and potentially full 3D nonlinear contact simulation,

would improve prediction accuracy in future work.

Despite these limitations, no evidence of structural instability, excessive deformation, or critical stress concentration was observed under nominal loading conditions.

Bearing and Seal Design and Selection

The bearing and sealing systems represent two of the most critical supporting subsystems within the radial piston hydraulic motor, as they directly govern mechanical stability, pressure containment, volumetric efficiency, and long-term operational reliability. While the cam-piston system defines the primary energy conversion mechanism, the bearings and seals ensure that this energy conversion occurs under controlled mechanical alignment and without excessive hydraulic loss.

In particular, the motor operates under combined radial, axial, and cyclic loading conditions, where both components are subjected to continuously varying forces arising from piston pressure events, cam contact reactions, and transient hydraulic pressure fluctuations. As such, both systems must be designed not only for static load capacity, but also for fatigue resistance, stiffness stability, and dynamic response under periodic excitation.

Bearing System

The bearing system performs several simultaneous roles within the motor architecture:

- supporting the rotating shaft under combined radial and axial loading,
- maintaining geometric alignment between cam ring and piston assemblies,
- preserving contact stability at the cam–roller interface,
- and minimising deflection-induced harmonic distortion.

Because the motor generates cyclic loading through discrete piston excitation events, the bearing system is subjected to both steady-state mean loads and oscillatory load components. These oscillatory loads arise from the phase-dependent variation in piston force contributions throughout the rotational cycle. Consequently, bearing performance must be evaluated in terms of:

- dynamic load capacity,
- stiffness under combined loading,
- fatigue life under cyclic excitation,

- and sensitivity to misalignment and deflection.

Bearing Selection Rationale

The final bearing configuration adopts tapered roller bearings (30205) conforming to ISO 355, with an internal shaft diameter of $d_b = 25\ mm$.

Tapered roller bearings were selected due to their inherent ability to support combined radial and axial loads within a single element. This is particularly important in cam-driven hydraulic systems, where the pressure angle between piston force vectors and shaft axis varies continuously throughout operation. Compared to alternative bearing types:

- Deep groove ball bearings provide simpler construction but limited axial load capacity.
- Cylindrical roller bearings provide high radial stiffness but require additional thrust support elements.
- Tapered roller bearings provide a balanced solution with high stiffness and combined load handling capability.

The selection is therefore driven by both load direction variability and the requirement for high positional stability under cyclic excitation.

Piston Force Transmission and Bearing Loading

Bearing loads originate primarily from piston reaction forces transmitted through the cam interface. For an individual piston, the hydraulic force is given by:

$$F_p = PA_p$$

where:

P is chamber pressure,
A_p is piston area.

This force resolves into tangential and radial components relative to the shaft axis:

$$F_t = F_p sin(\alpha)$$
$$F_r = F_p cos(\alpha)$$

where α represents the local pressure angle determined by cam geometry.

The tangential component contributes to torque generation, while the radial component contributes directly to shaft loading and therefore bearing reaction forces.

The total radial load acting on the bearing system is obtained by summing contributions from all active pistons:

$$F_{R_{total}} = \Sigma\, F_{r_i}$$

Due to the seven-piston, six-lobe coprime configuration, piston force contributions are phase-dispersed across the rotational cycle. This significantly reduces synchronous reinforcement of radial loads compared to non-coprime architectures, thereby lowering peak oscillatory bearing loading and improving fatigue performance.

This represents an important secondary structural benefit of the harmonic optimisation process: reductions in torque ripple directly translate into reductions in bearing load fluctuation amplitude.

Equivalent Bearing Load Model

For design evaluation, the time-varying bearing load is reduced to an equivalent dynamic load using the standard rolling bearing formulation:

$$P_e = XF_r + YF_a$$

where:

- P_e is the equivalent dynamic bearing load,
- F_r is radial load,
- F_a is axial load,
- X and Y are bearing-specific load factors determined by geometry.

For tapered roller bearings, axial load contribution is particularly significant due to the geometry of the rolling elements, which inherently convert radial loading into coupled thrust reactions.

Although the true loading is strongly time-dependent and periodic, the equivalent load approach provides a conservative design basis for fatigue life estimation and bearing sizing.

Bearing Life Estimation

Bearing fatigue life is evaluated using the standard L_{10} life formulation, representing the number of revolutions at which 90% of identical bearings are expected to survive under specified loading conditions.

The basic life equation is:

$$L_{10} = \left(\frac{C}{P_e}\right)^p$$

where:

- C is the dynamic load rating,
- P_e is the equivalent dynamic load,
- p is the life exponent.

For roller bearings:

$$p = \frac{10}{3}$$

The corresponding life in operating hours is given by:

$$L_{10,h} = \left(\frac{10^6}{60n}\right)\left(\frac{C}{P_e}\right)^p$$

where n is rotational speed in RPM.

For the operating condition of approximately 600 RPM, the calculated bearing life of $\approx 1.5\ yrs$ remains within acceptable limits for continuous operation under nominal loading conditions.

This confirms that the selected bearing system provides sufficient fatigue capacity for the intended design life, assuming proper lubrication and alignment maintenance.

Bearing Stiffness and Dynamic Stability

Beyond load capacity and fatigue life, bearing stiffness plays a critical role in maintaining system-level harmonic performance. Shaft deflection directly influences:

- cam–piston contact alignment,
- local pressure angle variation,
- leakage behaviour in piston bores,
- and the consistency of torque generation.

Excessive bearing compliance can introduce geometric misalignment, which in turn disrupts the harmonic optimisation achieved through the spline-based cam design.

The finite element analysis of the bearing support structure predicts a maximum deflection of:

$$\delta_{max} \approx 1.8 \times 10^{-2} mm \ (18\ microns)$$

This level of deformation is sufficiently small to preserve alignment between the cam ring, piston assemblies, and shaft axis under nominal operating conditions.

Corresponding strain levels remain low, indicating that the bearing support structure maintains adequate rigidity without approaching material yield limits.

Hydrostatic Lubrication and Film Effects

In addition to mechanical rolling contact, lubrication films within the piston-cylinder interfaces introduce hydrostatic and hydrodynamic support effects that influence both friction and load distribution.

The fluid film pressure distribution can be approximated using Reynolds equation:

$$\frac{\partial}{\partial x}\left(\frac{h^3 \partial p}{\partial x}\right) + \frac{\partial}{\partial y}\left(\frac{h^3 \partial p}{\partial y}\right) = 6\mu U \frac{\partial h}{\partial x}$$

where:

- h is film thickness,
- p is pressure,
- μ is dynamic viscosity,
- U is surface velocity.

This lubrication regime provides several important benefits:

- reduction of direct asperity contact,
- distributed load sharing across surfaces,
- damping of high-frequency mechanical oscillations,
- and improved wear resistance.

However, lubrication performance is strongly dependent on maintaining an appropriate balance between clearance, leakage, and pressure support. Excessively small clearances improve load support but increase friction and sensitivity to thermal expansion, while excessively large clearances reduce film stability and increase leakage losses.

The final design therefore adopts a balanced clearance regime that supports both hydrostatic stability and volumetric efficiency.

Sealing System Design

The sealing system is responsible for maintaining hydraulic pressure integrity while allowing controlled relative motion between moving components. Unlike static pressure vessels, the radial piston motor contains multiple dynamic interfaces, making perfect sealing physically unattainable. The primary functional requirements of the sealing system are:

- minimisation of volumetric leakage,
- maintenance of pressure containment under cyclic loading,
- tolerance of thermal expansion and structural deformation,
- and long-term wear resistance under lubrication exposure.

Rather than attempting to eliminate leakage entirely, the sealing design focuses on controlled leakage minimisation while preserving mechanical reliability and acceptable friction levels.

The final sealing system adopts a three-stage redundant architecture:

1. compressive C-channel primary seal,
2. PEEK O-ring secondary seal,
3. metallic V-type backup seal.

This layered configuration distributes sealing responsibility across multiple independent mechanisms, improving robustness against wear, deformation, and transient pressure spikes.

Primary C-Channel Seal

The primary sealing element is a compressive C-channel elastomeric seal that operates through elastic deformation under installation preload and hydraulic pressure.

The sealing pressure can be approximated as:

$$p_s = \frac{F_c}{A_c}$$

where:

- F_c is compressive force,
- A_c is effective contact area.

Effective sealing requires:

$$p_s > p_f$$

where p_f is the internal fluid pressure.

The C-channel geometry provides compliance under deformation, allowing it to accommodate:

- housing deformation under pressure,
- thermal expansion effects,

- and small manufacturing tolerances.

This compliance is essential for maintaining sealing integrity in a system where structural deformation, although small, is non-negligible.

Secondary PEEK O-Ring Seal

A secondary sealing stage is implemented using a PEEK-based O-ring to provide redundancy and enhanced chemical and thermal stability. PEEK is selected due to:

- high temperature resistance,
- low creep behaviour,
- excellent wear resistance,
- and strong chemical compatibility with hydraulic fluids.

The O-ring operates through radial compression, generating sealing stress proportional to elastic deformation:

$$\sigma_c \propto E\left(\frac{\delta}{d_o}\right)$$

where:

- E is elastic modulus,
- δ is compression displacement,
- d_o is O-ring diameter.

This secondary stage ensures continued sealing capability even in the event of partial degradation of the primary seal.

Metallic V-Type Backup Seal

The final sealing stage consists of a metallic V-type seal that provides structural sealing redundancy and mechanical alignment. Unlike polymeric seals, the metallic seal provides:

- high-pressure structural containment,
- geometric stability under deformation,
- and failure-resistant sealing behaviour.

Under increasing pressure, the sealing force increases proportionally:

$$F_n \propto PA_v$$

where A_v is the effective pressure-activated sealing area.

This pressure-assisted behaviour improves sealing effectiveness at higher operating pressures, making it particularly suitable as a final containment barrier.

Leakage Modelling and Trade-Offs

Leakage through narrow clearances is modelled using laminar flow approximation:

$$Q = \left(\frac{bh^3}{12\,\mu\,L}\right)\Delta P$$

This cubic dependence on clearance height highlights the extreme sensitivity of leakage to geometric tolerances. Even small increases in clearance can result in disproportionately large leakage increases. However, reducing clearance introduces competing constraints:

- increased frictional losses,
- higher risk of mechanical seizure,
- reduced tolerance to thermal expansion,
- and decreased lubrication film stability.

The final sealing and clearance design therefore represents a carefully balanced compromise between:

- leakage minimisation,
- mechanical reliability,
- lubrication stability,
- and manufacturability constraints.

Final Sealing System Assessment

Overall, the sealing architecture provides a robust multi-stage pressure containment system suitable for cyclic hydraulic operation under realistic conditions.

The combination of compliant, polymeric, and metallic sealing elements ensures that pressure integrity is maintained across a wide range of operating conditions while accommodating structural deformation, thermal variation, and wear progression.

Importantly, the sealing system is designed as a tolerant and redundant architecture rather than relying on a single high-precision sealing interface. This improves long-term reliability and reduces sensitivity to manufacturing variation, aligning the sealing design with the broader philosophy of physically robust optimisation used throughout the motor development process.

Materials Selection

Materials Selection and Tribological System Design

The material selection for the radial piston hydraulic motor is governed by the same coupled mechanical constraints identified in the structural and finite element analysis stages. In particular, the system operates under high-pressure cyclic loading, significant contact stress variation, and thermally induced dimensional changes. As a result, material selection cannot be treated independently for individual components but must instead be considered as part of an integrated tribological and structural system.

The dominant physical mechanisms influencing material performance include:

- Hertzian contact fatigue at cam–piston interfaces
- Sliding and rolling wear under mixed lubrication regimes
- Cyclic stress accumulation due to pressure ripple excitation
- Thermally induced expansion affecting clearance-dependent behaviour
- Corrosion and degradation in hydraulic fluid environments

Accordingly, the material selection strategy prioritises:

- Contact fatigue resistance over static strength alone
- Surface hardness gradients rather than homogeneous bulk hardness
- Dimensional stability under thermal and pressure cycling
- Compatibility with elastohydrodynamic lubrication (EHL) regimes
- Manufacturability under realistic machining and heat treatment constraints

This approach ensures consistency with the finite element results, where structural deformation was shown to remain small but non-negligible in regions critical to kinematic accuracy.

Cam Ring Material and Contact Interface Design

The cam ring represents the primary energy conversion interface within the motor, where hydraulic pressure is transformed into mechanical torque through rolling contact with piston-mounted rollers. This interface is governed predominantly by cyclic Hertzian contact stresses combined with sliding micro-motion, placing it within a fatigue-wear dominated failure regime. Identified failure mechanisms include subsurface fatigue crack initiation, surface pitting and spalling, adhesive wear under boundary lubrication, local plastic deformation under transient pressure spikes, and stiffness-induced distortion affecting kinematic accuracy.

Because the spline-based optimisation framework inherently seeks to minimize torque ripple by pushing local curvature radii to their physical limits, the cam ring material must tolerate aggressive geometric profiles. The finite element analysis of the cam ring indicates that elastic deformation remains extremely small under peak load conditions, with maximum displacement on the order of microns. However, even small geometric deviations are significant due to the system's reliance on precise harmonic cam geometry, reinforcing the requirement for high stiffness and fatigue resistance at the contact interface.

Selected material: AISI 4140 alloy steel (quenched, tempered, and surface hardened).

Justification: AISI 4140 provides a balanced combination of core toughness and surface hardness, making it suitable for components subjected to cyclic contact loading. The quenched and tempered core structure resists subsurface crack propagation, while surface hardening increases resistance to wear and pitting initiation. The hardened surface layer (50–60 HRC) ensures that contact stresses remain below the threshold for plastic deformation, while the tougher core absorbs cyclic energy without brittle failure. This material selection is consistent with the FEA results, which show that structural deformation is not the limiting factor; rather, long-term surface fatigue governs component lifespan.

Piston Structural and Tribological Design

The pistons function as pressure-loaded translating elements that convert hydraulic chamber pressure into normal force at the cam interface. Unlike the cam ring, which is primarily governed by contact fatigue, the piston experiences a more complex multiaxial stress state. Primary loading conditions include internal hydraulic pressure loading producing hoop stress, cyclic contact forces at the roller interface, inertial loading due to reciprocating acceleration, secondary bending stresses from cam reaction forces, and transient load spikes during valve switching events.

As identified in the nonlinear contact analysis, peak stress concentrations occur not strictly at the contact interface, but within adjacent piston wall regions due to bending moments. This reinforces the need for robust wall thickness design and smooth stress transitions.

Selected configuration: Nitrided alloy steel piston or bronze-coated steel piston.

Justification: Nitrided steels provide a hardened surface layer with high resistance to wear and scuffing while maintaining a ductile core for impact resistance. Alternatively, bronze coatings introduce a sacrificial wear layer that improves behaviour under lubrication degradation or transient boundary lubrication conditions. Both approaches are consistent with the observed mixed lubrication regime, where full film separation cannot be guaranteed during dynamic transient operation.

Housing and Structural Load Distribution System

The housing functions as the primary pressure containment structure and mechanical alignment framework for the entire motor assembly. Key loading sources include internal hydraulic pressure acting on chamber walls, reaction forces transmitted through piston-cam interactions, shaft and bearing reaction loads, and assembly preload stresses. Finite element analysis of the housing indicates that maintaining bore circularity and alignment is critical, as even small deviations can introduce uneven piston loading, leakage variations, and degradation of harmonic torque characteristics.

Material selection: Cast iron or hardened steel housing.

Justification: The modal analysis indicated a >10x separation between operating excitation frequencies and the first structural natural frequency (1073 Hz). Cast iron provides inherent damping characteristics that reduce vibration transmission and improve dynamic stability under cyclic loading, ensuring residual high-frequency ripple does not couple into external mounting points. Hardened steel alternatives provide higher strength and improved pressure resistance where weight or compactness constraints dominate, but the final selection prioritises a stiffness-to-damping balance.

Sealing System Design and Leakage-Control Architecture

The sealing system is treated as a coupled hydro-mechanical subsystem rather than a purely material selection problem. Its performance is governed by the interaction between pressure loading, structural deformation, and clearance-dependent leakage behaviour. Governing physical constraints dictate that leakage is highly sensitive to clearance variation, following a cubic relationship with gap height ($Q \propto h^3$). Furthermore, as established in the hydraulic dynamics modelling, leakage acts as a form of hydraulic damping; a zero-leakage design would increase hydraulic stiffness and potentially amplify pressure oscillations.

Because the FEA results demonstrated that the housing and cam ring experience non-negligible micron-level deformations under 450 bar loading, a single, tightly toleranced elastomeric seal would fail under this cyclic deformation or thermal expansion. To address these coupled constraints, a redundant three-stage sealing strategy is implemented:

1. **Primary elastomeric compression seal (C-channel geometry):** Operates through pressure-activated elastic deformation, providing adaptive sealing under structural variation, housing deformation, thermal expansion mismatch, and assembly tolerances.

2. **Secondary PEEK-based O-ring seal:** Implemented using PEEK due to its high thermal stability, low creep characteristics, and excellent chemical resistance to hydraulic fluids. This stage provides redundancy in the event of primary seal degradation and stabilises long-term performance under elevated thermal conditions.
3. **Metallic V-type backup seal:** Maintains geometric integrity under high stress and acts as a fail-safe pressure barrier. Its effectiveness increases with pressure ($F_n \propto PA_v$), providing a self-reinforcing sealing mechanism under peak load conditions.

Rather than relying on a single mechanism, this tolerant, multi-regime interface significantly reduces sensitivity to manufacturing variation, thermal distortion, wear progression, and transient pressure spikes, ensuring compatibility with the broader philosophy of structural robustness used throughout the motor design.

Summary of Integrated Material and Structural Design

The final material and subsystem design strategy is fundamentally driven by the results of the structural and finite element analysis. Across all components, the system demonstrates a consistent set of design drivers: contact-dominated fatigue governs cam–piston interfaces, pressure-driven deformation governs piston structural design, global stiffness governs housing performance, and clearance-sensitive leakage governs sealing architecture. Material selection is not treated as an isolated decision process, but as a direct response to the mechanical and thermal behaviour observed in the coupled system simulations, ensuring consistency across dynamic harmonic optimisation, structural deformation constraints, fatigue life predictions, and thermal and lubrication behaviour.

System Integration, Validation, and Operational Safety

System Integration and Validation

Following completion of the harmonic optimisation, structural validation, and subsystem design stages, the radial piston hydraulic motor was integrated into a full system-level simulation environment using Automation Studio. This stage serves as a system integration verification step, linking hydraulic dynamics, mechanical response, and electrical control logic into a single coupled representation of the motor operation.

The integrated model includes the following subsystems:

- Hydraulic pump (constant displacement source)
- Bidirectional radial piston hydraulic motor
- 4/3 directional control valve
- Pressure relief valve system and cross-port relief protection
- Hydraulic accumulator for transient stabilisation
- Return-line cooling and filtration system
- Pressure and flow sensing instrumentation
- Relay-based electrical control logic, solenoid-actuated directional control interface, and delay relay timing elements

The hydraulic and electrical domains are coupled through solenoid-driven actuation signals, allowing electrical relay logic to directly govern hydraulic flow direction and system state transitions. Simulation results confirm correct system-level behaviour under dynamic switching conditions: bidirectional motor operation was achieved without hydraulic instability, relay self-holding logic maintained stable state retention, emergency stop sequences successfully isolated system energy, electrical interlocking prevented simultaneous solenoid activation and hydraulic locking, and delay relays reduced transient pressure spikes during directional reversal. Importantly, the system-level response aligns with the transient behaviour predicted in the hydraulic dynamics analysis, particularly with respect to pressure ripple suppression and commutation stability.

Energy Balance and Efficiency Behaviour

The hydraulic power input was evaluated using measured simulation parameters: $P_h = pQ$ where: P_h is hydraulic power, p is system pressure, and Q is volumetric flow rate. Using representative operating conditions ($p \approx 450\ bar$, $Q \approx 180\ L/min$), the system power level is approximately 135 kW.

The energy losses observed in the simulation are distributed across multiple coupled mechanisms: valve throttling losses during directional switching, return-line pressure losses due to flow restriction, internal leakage within piston–cam interfaces, filtration-induced pressure drop, and thermal dissipation through cooling system operation. These losses reflect the coupled hydraulic–mechanical dissipation pathways identified in the earlier analysis. The open-centre valve configuration reduces idle-state energy consumption by enabling unloaded circulation, while the accumulator introduces system-level benefits by attenuating transient pressure spikes, smoothing pulsatile flow behaviour, and improving dynamic stability during switching events.

Thermal Behaviour and System Stability

Thermal behaviour was evaluated under sustained high-pressure operation conditions, where heat generation arises primarily from hydraulic throttling losses, internal leakage dissipation, viscous friction within fluid pathways, and transient switching losses. The simulation results indicate that thermal accumulation is a critical secondary effect of high-pressure operation. A return-line cooling system was therefore implemented to stabilise fluid temperature and maintain viscosity within acceptable operating bounds. The cooling system provides coupled benefits including reduced bulk oil temperature rise, improved viscosity stability and lubrication performance, reduced risk of elastomer seal degradation, and improved long-term structural and tribological reliability. The cooling system is additionally integrated into the electrical control logic, allowing thermal conditions to influence system-level operational safety constraints, confirming that steady-state operation can be maintained without progressive thermal runaway.

Safety Analysis and Operational Control Strategy

The hydraulic motor operates in a high-pressure, high-energy regime where failure modes are governed by the interaction between hydraulic storage energy, mechanical motion, thermal accumulation, and electrical control logic. The safety analysis therefore considers the system as a coupled energy domain network rather than isolated hazard categories.

Hydraulic Failure Modes: Operating at pressures approaching 450 bar represents significant stored hydraulic energy. Primary hazards include hose or fitting rupture under overpressure, transient pressure spikes due to rapid valve switching, cavitation, and accumulator discharge during maintenance. High-frequency pressure ripple introduces cyclic stress within piping, valve bodies, cam–piston interfaces, and structural housing elements, directly contributing to the fatigue mechanisms identified in the structural FEA section.

Mechanical Failure Modes: Hazards arise from rotational motion and dynamic load reversal, including sudden torque reversal, vibration-induced misalignment, and overspeed transients. If lubrication films degrade below the elastohydrodynamic regime threshold, direct asperity contact results in accelerated wear, increased frictional heating, and localised thermal distortion, leading to bearing fatigue, shaft cracking, and seal degradation.

Thermal and Electrical Failure Modes: Elevated oil temperatures result in reduced viscosity, accelerated seal degradation, increased leakage rates, and thermal expansion affecting critical clearances. Electrical hazards are primarily associated with control instability, particularly simultaneous energisation of forward/reverse solenoids, which may result in hydraulic locking and severe transient pressure spikes. This condition is mitigated through electrical interlocking logic, relay-based state control, and delayed actuation sequencing.

Risk Assessment Summary

The system-level risk assessment identifies key hazards and corresponding integrated mitigation strategies:

Table 4: Risk Assessment and Mitigation

Hazard	Potential Consequence	Risk Rating	Integrated Mitigation Measures
Hydraulic overpressure	Component rupture, fluid release, injury	**High**	Pressure relief valve, pressure monitoring, conservative design pressure margins
Pressure pulsation and ripple	Fatigue failure of pipes, fittings and seals	**Medium**	Hydraulic accumulator, damped pipe routing, compliant hose sections
Rapid valve switching (water hammer)	Pressure spikes, mechanical shock, accelerated wear	**Medium**	Controlled valve actuation timing, delay relay, soft switching strategy
Excessive operating temperature	Seal degradation, viscosity reduction, reduced component life	**Medium**	Heat exchanger, temperature monitoring, automatic shutdown on over-temperature
Solenoid or directional valve failure	Hydraulic locking, unintended actuator behaviour	**High**	Electrical interlocks, fail-safe valve configuration, fault detection logic
Rotating shaft and coupling	Entanglement or impact injury	**Medium**	Physical guarding, exclusion zones, lock-out/tag-out procedures

Elastohydrodynamic (EHL) film breakdown	Accelerated wear, scuffing and reduced efficiency	**Medium**	Lubrication management, appropriate surface finish, operating within design limits
Filter blockage or contamination	Cavitation, pump damage, reduced system performance	**Medium**	Differential pressure monitoring, scheduled filter replacement, contamination control
Residual accumulator pressure	Sudden fluid release during maintenance	**High**	Manual discharge valve, pressure indicator, documented depressurisation procedure
Electrical power or control fault	Unintended operation or loss of control	**Medium**	Emergency stop circuit, fused power distribution, fail-safe controller design

Mitigation strategies are implemented as system-level constraints rather than isolated protections: pressure relief valves regulate overpressure, accumulators stabilise transient fluctuations, delay relays reduce shock loads, electrical interlocks prevent unsafe states, the open-centre configuration reduces idle pressure, and thermal feedback control regulates the operating envelope.

Standard Operating Procedure (SOP)

The operational procedure is defined to ensure controlled energy management throughout system operation.

Pre-start verification: Verify hydraulic fluid level and condition, system integrity (hoses, fittings, seals), accumulator pre-charge state, electrical power availability, filter condition and restriction status, cooling system functionality, emergency stop operability, and absence of leakage or mechanical damage.

Start-up sequence: Confirm neutral valve position, energise control system, verify emergency stop readiness, start hydraulic pump, allow pressure stabilisation, initiate forward or reverse command via control input, and monitor pressure, vibration, and temperature response.

Normal operation: Monitor pressure stability and ripple behaviour, monitor oil temperature and thermal drift, observe vibration and acoustic response, prevent rapid directional switching, and maintain cooling system operation.

Shutdown procedure: Return directional valve to neutral, stop hydraulic pump, de-energise control system, isolate electrical supply, and release residual hydraulic pressure if maintenance is required.

Emergency shutdown: Immediately activate emergency stop, de-energise all control logic, return directional valve to neutral state, cease hydraulic flow, and ensure full system energy isolation prior to inspection. Accumulator pressure must be verified as discharged before maintenance operations commence.

Discussion and Engineering Trade-offs

The results of the mathematical modelling, harmonic analysis, optimisation process, and structural evaluation collectively demonstrate that the design of a radial piston hydraulic motor is fundamentally governed by a series of tightly coupled engineering trade-offs. While the optimisation framework developed in this work provides a systematic method for exploring the design space, the achievable performance of the motor ultimately remains constrained by the underlying physical behaviour of the hydraulic, mechanical, structural, and manufacturing systems.

The preceding analyses demonstrated that torque ripple, pressure pulsation, structural loading, cavitation behaviour, efficiency, and manufacturability are not independent objectives. Improvements achieved within one performance domain frequently introduce penalties elsewhere within the coupled system. Consequently, the design process cannot be approached as the isolated optimisation of individual parameters, but rather as the coordinated balancing of competing physical constraints across multiple interacting subsystems.

The final seven-piston, six-lobe architecture emerged not from arbitrary geometric selection, but from the interaction between harmonic smoothness requirements, contact mechanics limitations, hydraulic stability considerations, manufacturability constraints, and long-term operational reliability. The following discussion synthesises these competing effects and interprets the broader engineering implications of the modelling and optimisation results presented throughout this work.

Harmonic Architecture Versus Mechanical Realisability

One of the most significant findings of the harmonic analysis is that the piston-lobe architecture itself acts as a first-order determinant of dynamic smoothness before any geometric optimisation is introduced. The earlier architectural investigations demonstrated that coprime piston-lobe combinations inherently suppress coherent low-order harmonic reinforcement through phase dispersion behaviour. By preventing repeated synchronous alignment between pistons and cam lobes, excitation energy becomes distributed more uniformly throughout the rotational cycle rather than concentrating within dominant low-frequency oscillation modes.

This behaviour explains why the seven-piston, six-lobe architecture consistently emerged as one of the most favourable configurations during the preliminary design investigations. The 7/6 arrangement produced strong harmonic dispersion characteristics while simultaneously maintaining practical geometric proportions and acceptable mechanical loading behaviour.

However, harmonic smoothness alone cannot determine the suitability of a motor architecture. Increasing piston count improves overlap smoothness and reduces the magnitude of individual pressure impulses but simultaneously introduces several significant mechanical penalties. For a fixed housing diameter, increasing piston count reduces the available bore area for each cylinder, increasing leakage sensitivity, reducing wall thickness between adjacent bores, tightening manufacturing tolerances, and complicating assembly requirements. Closely packed cylinders additionally increase structural stress concentration within the housing and reduce robustness to machining variation.

Similarly, increasing cam lobe count raises the effective excitation frequency and improves overlap continuity between adjacent pistons, but also reduces the local radius of curvature of the cam surface. Smaller curvature radii increase piston acceleration gradients, elevate

Hertzian contact stress, increase roller loading, and worsen lubrication conditions at the cam interface. Excessively aggressive lobe geometries may additionally introduce undercutting behaviour and non-manufacturable surface curvature transitions.

Conversely, architectures employing very low piston or lobe counts generally exhibit mechanically simpler geometries and larger piston areas but produce substantially stronger low-order torque oscillation and pressure pulsation behaviour. These low-frequency oscillations couple strongly into the rotational inertia of the drivetrain and are only weakly attenuated by hydraulic compressibility and structural damping.

The architectural selection process therefore becomes a balance between harmonic smoothness, contact mechanics, achievable piston area, structural integrity, packaging practicality, and manufacturability. The final 7/6 configuration emerged as a favourable compromise because it simultaneously provided strong harmonic dispersion, moderate pressure-angle behaviour, acceptable curvature distributions, practical cylinder spacing, and mechanically stable contact conditions without requiring excessively aggressive geometric shaping during optimisation.

Cam Profile Freedom Versus Contact Stress and Manufacturability

The cam-ring architecture adopted in this work provides substantial geometric freedom for harmonic optimisation and ripple suppression. This flexibility is one of the primary advantages of cam-driven radial piston motors because the cam profile directly governs piston displacement, chamber volume evolution, piston acceleration behaviour, and therefore the resulting torque waveform.

However, this geometric freedom also introduces several competing mechanical constraints. Aggressive local shaping of the cam profile may reduce simulated torque ripple while simultaneously generating undesirable physical behaviour elsewhere within the system. Excessive curvature gradients increase piston acceleration and jerk, which in turn elevate inertial loading, roller contact force variation, lubrication film instability, and local Hertzian stress concentration. Sharp local curvature transitions may additionally worsen pressure-angle behaviour and increase side loading within the piston-cylinder interfaces.

These effects become particularly important during optimisation because unconstrained mathematical optimisers naturally attempt to exploit high-frequency geometric oscillations in order to artificially suppress instantaneous ripple metrics. Earlier Fourier-based optimisation investigations demonstrated this behaviour directly, producing geometries containing narrow high-frequency curvature oscillations which numerically reduced torque ripple while simultaneously generating unrealistic contact conditions, unstable piston acceleration behaviour, and non-manufacturable surfaces.

The adoption of periodic B-spline parameterisation substantially improved this behaviour by restricting the optimiser to smoother and more physically realistic geometric modes. The addition of smoothness regularisation and jerk penalty constraints further prevented the optimisation framework from exploiting unrealistic curvature oscillation.

The resulting trade-off is therefore between geometric freedom for harmonic shaping and the mechanical limitations imposed by contact stress, lubrication stability, surface manufacturability, and dynamic piston behaviour. The optimisation process cannot simply minimise ripple magnitude in isolation; it must simultaneously maintain mechanically feasible curvature distributions and stable dynamic behaviour throughout the rotational cycle.

Hydraulic Dynamics Versus Efficiency and Stability

The hydraulic subsystem introduces another set of tightly coupled trade-offs involving pressure dynamics, compressibility, leakage behaviour, and flow stability. Chamber pressure evolution depends fundamentally upon the interaction between piston-induced volume change, valve timing, leakage flow, and fluid compressibility. Consequently, parameters that improve one aspect of hydraulic performance frequently degrade another.

Increasing the effective bulk modulus of the hydraulic fluid increases hydraulic stiffness and improves transient torque response by reducing compliance within the chamber system. However, reduced compressibility also weakens the damping effect provided by the fluid, potentially amplifying high-frequency pressure transients and increasing susceptibility to cavitation during rapid commutation events.

Similarly, larger port areas reduce throttling losses and improve chamber filling behaviour, but may simultaneously generate sharper pressure equalisation events, larger flow-induced oscillations, and more severe commutation shock during valve transition. Smaller port areas improve transition smoothness but increase pressure drop and volumetric loss.

Clearance geometry introduces additional compromises. Tighter piston clearances reduce leakage and improve volumetric efficiency, but increase friction sensitivity, reduce tolerance to thermal expansion and contamination, and increase manufacturing difficulty. Larger clearances improve robustness and lubrication stability but increase leakage flow and reduce effective damping within the hydraulic system.

Importantly, leakage itself plays a dual role within the motor behaviour. While excessive leakage reduces efficiency and pressure support capability, leakage also acts as a form of hydraulic damping. Extremely low leakage may therefore reduce dissipation and increase susceptibility to oscillatory pressure behaviour within the coupled hydraulic-mechanical system.

These competing effects illustrate that efficiency, pressure stability, cavitation suppression, and dynamic smoothness cannot be optimised independently. The optimisation framework therefore incorporates combined spectral, leakage, and efficiency terms in order to balance these competing behaviours within a unified objective formulation.

Piston Inertia Versus Dynamic Stability

The coupled hydraulic-mechanical behaviour of the motor may be interpreted as a mass-spring-damper system in which piston inertia acts as the mass element, fluid compressibility provides effective hydraulic stiffness, and leakage together with viscous losses contribute damping behaviour.

This interpretation reveals another important engineering trade-off involving piston mass and dynamic response. Increasing piston mass improves robustness to high-frequency disturbances and reduces sensitivity to local geometric irregularities but simultaneously increases inertial loading at the cam interface and reduces transient responsiveness. Larger inertial forces also increase roller contact loading and structural stress within the piston support regions.

Conversely, reducing piston mass improves responsiveness and reduces inertial contact loading, but may increase susceptibility to oscillatory behaviour when combined with high hydraulic stiffness. Excessively low piston inertia may additionally increase sensitivity to high-frequency excitation originating from valve commutation and local curvature variation, potentially introducing dynamic amplification behaviour within the coupled hydraulic-mechanical system.

The resulting stability behaviour depends strongly on the interaction between piston mass, hydraulic stiffness, damping ratio, and excitation frequency. Designs possessing excessively high stiffness or insufficient damping may enter underdamped operating regimes in which pressure ripple and torque ripple reinforce one another dynamically.

The optimisation process must therefore maintain an appropriate balance between responsiveness, stability, contact loading, and damping behaviour in order to preserve smooth operation throughout the rotational cycle.

Leakage, Tolerances, and Long-Term Reliability

Several important trade-offs additionally emerge when considering practical manufacturing tolerances and long-term operational behaviour. The reduced-order simulation model assumes idealised geometry and simplified leakage behaviour; however, real hydraulic machinery inevitably contains geometric variation arising from machining tolerances, surface roughness, assembly misalignment, bearing clearances, thermal deformation, and progressive wear.

These effects strongly influence the long-term stability of the motor. Tighter manufacturing tolerances generally improve efficiency, reduce leakage, and improve harmonic smoothness, but also increase production cost, reduce tolerance to contamination, and increase sensitivity to thermal expansion and assembly variation. Extremely tight clearances may additionally destabilise lubrication films and increase seizure risk under transient operating conditions.

Conversely, looser tolerances improve manufacturability, assembly robustness, and wear tolerance, but increase leakage flow, reduce volumetric efficiency, and potentially worsen pressure ripple behaviour through uneven piston loading and increased chamber pressure variation.

Wear progression introduces further complexity because the operating characteristics of the motor evolve throughout service life. Progressive wear generally increases leakage and reduces hydraulic stiffness while simultaneously altering damping behaviour, piston alignment, and contact conditions. Consequently, a motor which performs favourably under idealised initial conditions may exhibit degraded harmonic and efficiency behaviour over extended operation.

The final design must therefore remain dynamically stable and mechanically robust not only under nominal conditions, but across the full tolerance envelope and throughout long-term wear progression.

Optimisation Capability Versus Physical Constraints

The hybrid Bayesian optimisation framework developed in this work proved highly effective for navigating the nonlinear and strongly coupled design space associated with radial piston motor optimisation. The surrogate-based optimisation strategy substantially improved search efficiency while enabling the exploration of complex interactions between geometry, valve timing, hydraulic dynamics, and harmonic behaviour.

However, the optimisation process itself remains fundamentally constrained by the underlying physics of the system. Optimisation algorithms cannot compensate indefinitely for poor architectural choices or physically unfavourable geometry. As demonstrated throughout the earlier architectural analysis, poor piston-lobe configurations force the optimiser toward increasingly aggressive geometric shaping in an attempt to artificially suppress harmonic excitation.

Such behaviour frequently produces elevated contact stress, unstable piston acceleration, unrealistic curvature distributions, and physically impractical geometries. Although these solutions may occasionally appear favourable numerically, they remain mechanically infeasible and dynamically unstable in practice.

The optimisation framework therefore functions most effectively when applied to an architecture that already possesses favourable underlying harmonic characteristics. In this work, the seven-piston, six-lobe arrangement provided such a baseline, allowing the optimisation process to refine the geometry rather than attempting to compensate for fundamentally poor harmonic behaviour.

This distinction is important because it reinforces a broader engineering principle: optimisation should enhance a physically sensible architecture rather than attempt to rescue an inherently flawed design.

Model Fidelity Versus Computational Tractability

In addition to the physical trade-offs embedded within the motor architecture itself, further compromises arise from the modelling strategy required to enable practical optimisation.

The reduced-order mathematical model intentionally simplifies several complex physical phenomena, including nonlinear leakage behaviour, transient pressure-wave propagation, structural elasticity, multiphase cavitation dynamics, temperature-dependent fluid properties, valve plate dynamics, and detailed turbulence effects. These simplifications substantially reduce computational cost and enable rapid optimisation across large regions of the design space.

However, increased computational efficiency is achieved at the expense of predictive fidelity. High-fidelity CFD and fully coupled nonlinear finite element simulations would provide more accurate local flow and stress predictions but would be computationally impractical within an iterative optimisation framework involving thousands of candidate evaluations.

The selected modelling approach therefore represents a compromise between physical realism and optimisation tractability. The reduced-order framework captures the dominant hydraulic and harmonic behaviour required for meaningful early-stage design exploration while remaining computationally manageable for surrogate-assisted optimisation.

Nevertheless, the resulting simulations should not be interpreted as a complete digital twin of the physical motor. Final validation of the design ultimately requires higher-fidelity CFD analysis, nonlinear structural simulation, experimental testing, and long-duration durability evaluation.

Summary of Engineering Trade-offs

The analyses presented throughout this work collectively demonstrate that the behaviour of a radial piston hydraulic motor emerges from the interaction of multiple tightly coupled physical systems rather than from any isolated design parameter.

Architectural modifications that improve harmonic smoothness frequently increase geometric complexity, contact stress, and manufacturing sensitivity. Changes intended to improve efficiency may simultaneously reduce damping, thermal robustness, or lubrication stability. Increasing geometric freedom improves harmonic shaping capability but also increases the risk of non-physical curvature distributions and unstable dynamic behaviour. Similarly, tighter clearances improve volumetric efficiency while simultaneously increasing sensitivity to wear, contamination, and thermal expansion.

No single parameter can therefore be maximised independently without introducing penalties elsewhere within the system. The final design solution instead emerges from the balancing of competing objectives across harmonic behaviour, hydraulic stability, structural durability, manufacturability, efficiency, and long-term operational robustness.

Overall Interpretation

Overall, the results of this work demonstrate that the cam-ring radial piston hydraulic motor represents a constrained multi-objective equilibrium between harmonic smoothness, hydraulic stability, structural durability, efficiency, manufacturability, and long-term operational reliability.

The selected seven-piston, six-lobe architecture provided an inherently favourable harmonic foundation which enabled the optimisation framework to refine the motor geometry without resorting to unrealistic or mechanically unstable solutions. The spline-based parameterisation successfully constrained the optimisation process to physically plausible geometric modes while preserving sufficient flexibility for meaningful harmonic shaping.

The reduced-order physics framework captured the dominant coupled hydraulic-mechanical behaviour required for optimisation while remaining computationally tractable for large-scale surrogate-assisted exploration. Although several simplifying assumptions remain present within the model, the combined simulation, optimisation, and structural analyses indicate that the resulting motor geometry is both dynamically realistic and mechanically feasible within the intended operating regime.

Most importantly, the work demonstrates that meaningful improvement in radial piston motor behaviour is achieved not through isolated optimisation of individual parameters, but through coordinated management of the coupled harmonic, hydraulic, structural, thermal, and manufacturing constraints that govern the system as a whole.

Future Improvements and Next Steps

The work completed throughout this project established a strong foundation for the systematic design and optimisation of a high-performance radial piston hydraulic motor. The investigation demonstrated the importance of integrating harmonic analysis, hydraulic modelling, structural evaluation, and practical engineering constraints within a unified design methodology. Through the selection of a harmonically favourable cam-ring architecture and the identification of an optimal seven-piston, six-lobe configuration, the project developed a mechanically realistic motor concept capable of improved torque smoothness, structural stability, and hydraulic performance. More importantly, it established a physically grounded framework linking geometric architecture directly to system-level behaviour, enabling design decisions to be made on the basis of measurable performance outcomes rather than intuition alone.

Although the current approach provides meaningful insight into the dominant system behaviour and key engineering trade-offs, several targeted improvements could significantly enhance both design quality and predictive capability by reducing modelling uncertainty and increasing the resolution of geometry optimisation.

A primary limitation of the current framework is the reliance on reduced-order contact and structural models, which necessarily approximate the local behaviour of the cam–roller interface. Improving contact mechanics resolution through higher-fidelity nonlinear simulation would reduce uncertainty in peak Hertzian stress prediction at the cam surface. In practical terms, this would allow the minimum cam radius and fillet transitions to be reduced without exceeding stress limits, enabling a more aggressive curvature profile. This would directly improve harmonic smoothness by allowing finer shaping of the cam function without requiring conservative geometric smoothing to maintain structural safety.

Similarly, improved modelling of leakage and clearance flow would directly influence piston and sealing design. At present, leakage behaviour is represented using simplified analytical relations, which do not fully capture transient effects, surface roughness interaction, or wear evolution. A higher-fidelity fluid model would reduce uncertainty in predicted volumetric efficiency, allowing tighter clearance specifications without excessive risk of seizure or performance degradation. This would improve overall efficiency while also reducing sensitivity to manufacturing variation assumptions.

Thermal–hydraulic coupling is another area where improved modelling would directly affect design outcomes. More accurate prediction of temperature distribution would allow seal compression behaviour, fluid viscosity variation, and clearance expansion to be modelled more realistically. This would enable more reliable sizing of sealing elements and reduce conservative over-design driven by worst-case thermal assumptions. In turn, this would improve long-term efficiency stability and reduce performance drift under continuous operation.

Beyond physics modelling improvements, a significant opportunity exists in the optimisation architecture itself. The current hybrid approach, based on Gaussian Process regression combined with Bayesian optimisation, provides an efficient framework for exploring the design space. However, future development would benefit from a more advanced optimisation pipeline that improves both exploration efficiency and physical consistency. In particular, integrating Physics-Informed Neural Networks (PINNs) would allow physical constraints such as conservation laws and pressure continuity to be embedded directly into the surrogate model, reducing reliance on purely data-driven interpolation in poorly sampled regions.

Coupling this with uncertainty-aware Gaussian Process modelling would ensure that exploration is guided not only by predicted performance but also by confidence bounds, improving robustness in high-risk design regions such as extreme curvature or high pressure-angle transitions. Extending the acquisition strategy using reinforcement learning methods such as Soft Actor-Critic (SAC) would further improve sequential decision-making efficiency by learning optimal sampling policies rather than relying on fixed acquisition heuristics. When combined, this hybrid PINN + GP + SAC framework would improve convergence speed and reduce the number of expensive evaluations required to identify high-performance regions of the design space.

Importantly, the value of this improved optimisation architecture is not purely computational efficiency, but its direct impact on design resolution. Faster and more accurate evaluation would allow a significantly denser exploration of cam profile variations, enabling finer control over curvature gradients, pressure-angle transitions, and piston timing. This would translate directly into smoother torque output, reduced contact loading variation, and improved hydraulic efficiency, rather than simply improving model performance in isolation.

In parallel, increased computational capability through GPU acceleration (CUDA-based processing) would further amplify these benefits by enabling parallel evaluation of multiple design candidates and operating conditions. This would make it feasible to perform high-resolution optimisation of cam geometry and transient operating behaviour simultaneously, rather than sequentially, significantly improving overall design throughput.

A further important improvement pathway lies in transitioning from reduced-order modelling toward a more complete multi-physics digital twin of the motor system. While the current model captures the dominant system dynamics, a digital twin would enable fully coupled simulation of hydraulic, structural, thermal, and tribological behaviour. The primary design impact of such a model would be improved confidence in local behaviour predictions, particularly in regions where current assumptions introduce conservative design constraints. This would allow tighter geometric tolerances and more aggressive optimisation of performance-critical features such as cam curvature, piston clearance, and sealing interfaces.

Beyond computational improvements, experimental validation remains essential for ensuring that simulated behaviour corresponds to real operating conditions. A physical prototype would enable direct measurement of torque ripple, pressure pulsation, vibration, thermal response, and volumetric efficiency. This would provide a direct feedback mechanism for refining modelling assumptions, particularly in areas such as leakage behaviour, contact fatigue, and wear progression, which are difficult to fully capture in early-stage simulation. Experimental data would also enable calibration of model parameters, reducing uncertainty in long-term performance prediction.

Manufacturing considerations represent another key area for future refinement. While the current design is geometrically optimised within a theoretical framework, real-world implementation introduces constraints associated with machining tolerance, surface finish, assembly alignment, and material treatment. Improving modelling resolution in these areas would allow better prediction of tolerance sensitivity, particularly in cam profile accuracy, piston bore concentricity, and sealing surface flatness. This would reduce the gap between simulated and manufactured performance, ensuring that optimisation outcomes remain achievable in practice.

Thermal effects also warrant further integration into the design process, as temperature variations directly influence fluid viscosity, leakage rates, seal deformation, and lubrication film thickness. Improved thermal–hydraulic coupling would allow more accurate prediction of efficiency variation under sustained load, as well as improved sizing of cooling requirements and sealing systems. This would reduce conservative thermal safety margins and improve long-term operating stability.

Finally, there is scope for incorporating active control strategies to complement the mechanically optimised architecture. Techniques such as adaptive commutation timing, pressure-feedback flow control, and active damping could be used to further reduce residual torque ripple and improve dynamic response under variable loading conditions. These control-based enhancements would act as secondary performance refinements, building upon the inherently smooth behaviour of the optimised cam–piston geometry rather than replacing it.

Overall, the future development pathway focuses on progressively reducing modelling uncertainty and increasing the resolution of geometry-level optimisation, rather than changing the fundamental design approach. Each proposed improvement directly translates into a specific engineering benefit: improved contact modelling enables more aggressive cam curvature design, improved leakage prediction enables tighter clearances and higher efficiency, thermal coupling improves sealing reliability and long-term stability, and enhanced optimisation architecture enables finer and more reliable shaping of the cam profile. Together, these developments would allow the current concept to evolve from a robust theoretical design into a highly refined, manufacturable, and industrially competitive hydraulic motor.

Conclusion

The design of a radial piston hydraulic motor is governed by the interaction between harmonic behaviour, hydraulic dynamics, structural durability, manufacturability, and long-term operational stability. Throughout this project, it has been demonstrated that achieving a smooth, efficient, and mechanically robust hydraulic motor cannot be accomplished through isolated optimisation of individual parameters. Instead, successful motor design requires the careful balancing of multiple competing engineering constraints, where improvements in one area frequently introduce compromises in another. The resulting motor architecture therefore emerged not from the pursuit of a single optimal metric, but from the development of a mechanically coherent and harmonically favourable system capable of maintaining stable performance under realistic operating conditions.

The comparative architectural investigation established the cam-ring radial piston configuration as the most suitable foundation for the design objectives considered in this work. While eccentric, crankshaft-driven, and phased-rotor arrangements each offer certain advantages, the cam-ring architecture uniquely combines harmonic controllability, structural simplicity, geometric flexibility, and mechanical robustness within a single system. Its continuous cam profile enables direct control over piston displacement behaviour, allowing torque ripple characteristics, pressure evolution, and piston phasing to be shaped with substantially greater precision than alternative architectures. At the same time, the configuration avoids many of the synchronisation challenges, packaging difficulties, and mechanical complexities associated with more aggressive multi-rotor systems. This combination of controllable geometry and practical mechanical feasibility made the cam-ring arrangement the most appropriate basis for optimisation and structural refinement.

The harmonic analysis further demonstrated the importance of selecting a favourable piston–lobe relationship prior to detailed geometric optimisation. Coprime piston–lobe combinations were shown to distribute excitation energy more uniformly throughout the rotational cycle and suppress low-order harmonic reinforcement. In particular, the selected seven-piston, six-lobe configuration exhibited substantially improved harmonic behaviour compared to non-coprime alternatives, reducing synchronous torque reinforcement without requiring excessive geometric distortion of the cam profile. This proved to be a critical design outcome because it established a mechanically realistic optimisation foundation. Rather than forcing the optimisation framework to compensate for fundamentally poor harmonic architecture through aggressive cam shaping, the selected configuration naturally supported smoother torque generation and more stable pressure evolution from the outset.

The optimisation framework subsequently demonstrated that meaningful improvements in motor smoothness and dynamic behaviour can be achieved when harmonic reasoning is combined with physically informed geometric constraints. The spline-based cam parameterisation provided sufficient design freedom to refine piston motion while simultaneously preserving manufacturable curvature distributions and mechanically stable contact behaviour. Importantly, the work showed that harmonic performance cannot be considered independently from structural and hydraulic behaviour. Excessively aggressive cam shaping may reduce certain harmonic components, but it also increases pressure angle variation, contact stress, roller acceleration, and manufacturing difficulty. The inclusion of curvature constraints, smoothness penalties, and physically motivated objective functions therefore played a critical role in ensuring that the optimisation process converged toward mechanically realistic solutions.

The hydraulic modelling additionally highlighted the interconnected nature of pressure dynamics, volumetric efficiency, leakage behaviour, and system stability. Chamber pressure evolution was shown to depend strongly on the balance between inflow, piston-induced volume variation, and leakage flow, with fluid compressibility acting as a dominant source of dynamic stiffness within the system. Increasing hydraulic stiffness improves transient responsiveness but also amplifies pressure ripple and cavitation sensitivity. Similarly, tighter clearances improve volumetric efficiency while simultaneously increasing sensitivity to thermal expansion, contamination, and manufacturing tolerances. These competing effects demonstrate that hydraulic motor performance is fundamentally governed by engineering compromise rather than absolute optimisation. Stable and efficient operation requires the simultaneous balancing of leakage control, lubrication stability, dynamic response, and manufacturability.

The structural and finite element analyses further demonstrated that the selected architecture remains mechanically feasible within the intended operating regime. Contact stress analysis, fatigue evaluation, modal analysis, and bearing support simulations collectively indicated that the motor possesses acceptable stiffness, deformation behaviour, and fatigue resistance for preliminary structural validation. The relatively small, predicted deflections suggest that the optimised harmonic behaviour is unlikely to be significantly degraded through elastic deformation during operation. Likewise, the separation between the dominant operating excitation frequencies and the primary structural modes indicates favourable dynamic stability and reduced resonance risk. Although additional refinement through higher-fidelity nonlinear modelling and experimental testing would further improve predictive accuracy, no major structural instabilities or catastrophic stress concentrations were identified within the analysed loading conditions.

The bearing and sealing system design also demonstrated the importance of integrating supporting subsystems into the overall optimisation philosophy. The use of tapered roller bearings provided sufficient stiffness and combined radial-axial load capacity to maintain shaft alignment and preserve piston contact stability under cyclic loading. Similarly, the layered sealing arrangement balanced leakage reduction, hydrostatic lubrication support, manufacturability, and long-term durability rather than relying on unrealistic zero-leakage assumptions. These supporting systems are not secondary additions to the motor architecture; they directly influence harmonic smoothness, efficiency, wear progression, and long-term operational reliability.

A major outcome of this work is the demonstration that optimisation alone cannot compensate for fundamentally poor architecture. Reduced-order optimisation frameworks are highly effective when applied to physically favourable configurations, but they remain constrained by the underlying mechanical and hydraulic realities of the system. Poor piston–lobe relationships, excessive curvature demands, or mechanically unstable geometries cannot be fully corrected through numerical optimisation alone. Consequently, successful hydraulic motor design depends first on the establishment of strong architectural foundations that naturally support favourable harmonic and structural behaviour before refinement and optimisation are applied.

Overall, this project demonstrates that the successful design of a radial piston hydraulic motor requires the integration of harmonic analysis, hydraulic modelling, structural mechanics, and practical engineering judgement within a unified design methodology. The selected seven-piston, six-lobe cam-ring architecture provides a mechanically realistic and harmonically favourable foundation capable of supporting smooth torque generation, acceptable structural durability, and stable hydraulic behaviour. By combining physically informed optimisation with practical engineering constraints, the resulting motor concept achieves a balanced compromise between efficiency, smoothness, manufacturability, and long-term reliability.

Ultimately, the work establishes a coherent and mechanically feasible framework for the design and optimisation of advanced radial piston hydraulic motors. Rather than treating harmonic smoothness, structural durability, and hydraulic efficiency as isolated design objectives, the project demonstrates the importance of considering these behaviours as strongly coupled aspects of a unified engineering system. This integrated design philosophy provides a robust basis for the continued development of high-performance hydraulic actuation systems capable of achieving improved smoothness, efficiency, durability, and operational stability within practical engineering constraints.